© 2019. Published by The Company of Biologists Ltd | Journal of Cell Science (2019) 132, jcs234799. doi:10.1242/jcs.234799

RESEARCH ARTICLE

The spindle pole body of *Aspergillus nidulans* is asymmetrical and contains changing numbers of γ-tubulin complexes

Xiaolei Gao[1], Marjorie Schmid[1], Ying Zhang[1], Sayumi Fukuda[2], Norio Takeshita[2] and Reinhard Fischer[1,*]

ABSTRACT

Centrosomes are important microtubule-organizing centers (MTOCs) in animal cells. In addition, non-centrosomal MTOCs (ncMTOCs) are found in many cell types. Their composition and structure are only poorly understood. Here, we analyzed nuclear MTOCs (spindle-pole bodies, SPBs) and septal MTOCs in *Aspergillus nidulans*. They both contain γ-tubulin along with members of the family of γ-tubulin complex proteins (GCPs). Our data suggest that SPBs consist of γ-tubulin small complexes (γ-TuSCs) at the outer plaque, and larger γ-tubulin ring complexes (γ-TuRC) at the inner plaque. We show that the MztA protein, an ortholog of the human MOZART protein (also known as MZT1), interacted with the inner plaque receptor PcpA (the homolog of fission yeast Pcp1) at SPBs, while no interaction nor colocalization was detected between MztA and the outer plaque receptor ApsB (fission yeast Mto1). Septal MTOCs consist of γ-TuRCs including MztA but are anchored through AspB and Spa18 (fission yeast Mto2). MztA is not essential for viability, although abnormal spindles were observed frequently in cells lacking MztA. Quantitative PALM imaging revealed unexpected dynamics of the protein composition of SPBs, with changing numbers of γ-tubulin complexes over time during interphase and constant numbers during mitosis.

This article has an associated First Person interview with the first author of the paper.

KEY WORDS: *Aspergillus*, Microtubules, γ-tubulin, MTOC, SPB, GCP, MOZART

INTRODUCTION

Microtubules (MTs) play essential roles in eukaryotic cells in many cellular processes, such as mitosis, protein and organelle transportation and cell polarity establishment. They are nucleated from large protein complexes called microtubule-organizing centers (MTOCs). The centrosome is a prominent MTOC in animal cells. Centrosomes organize the mitotic spindle and also polymerize cytoplasmic MTs in certain interphase cells. However, many – if not all – cell types employ non-centrosomal MTOCs (ncMTOCs) after differentiation to produce cell-type-specific MT arrays (Tillery et al., 2018). Whereas centrosomes are studied very well, the structure and function of ncMTOCs is in its infancy. The filamentous fungus *Aspergillus nidulans* has spindle pole bodies (SPBs), the functional analogs of centrosomes, and septum-associated MTOCs (sMTOCs) as ncMTOCs (Konzack et al., 2005; Oakley, 2004; Oakley et al., 2015; Oakley and Oakley, 1989; Zekert et al., 2010; Zhang et al., 2017). Thus, *A. nidulans* is a great model to study different MTOC types in differentiated cells.

The key component of MTOCs is γ-tubulin, which was first identified in *A. nidulans* (Oakley and Oakley, 1989), and later in fission yeast, animals, human and plants (Horio and Oakley, 2003; Horio et al., 1991; Julian et al., 1993; Liu et al., 1994). Together with the γ-tubulin complex proteins (GCPs, also known as TUBGCPs in mammals), GCP2–GCP6, it functions as an MT nucleation template. This large complex is termed the γ-tubulin ring complex (γ-TuRC) based on its highly ordered three-dimensional ring-like structure (Moritz et al., 2000; Zheng et al., 1995).

Three components, γ-tubulin, GCP2 and GCP3, constitute the core structure of the γ-TuRC and are termed the γ-tubulin small complex (γ-TuSC) (Kollman et al., 2010). The γ-TuSC proteins are essential in all eukaryotic cells, and *Saccharomyces cerevisiae* only contains γ-TuSCs (Colombié et al., 2006; Knop and Schiebel, 1997; Martin et al., 1998; Oegema et al., 1999; Vardy and Toda, 2000; Xiong and Oakley, 2009). γ-TuSC itself can self-assemble into a ring structure facilitating MT nucleation, although with lower efficiency than the γ-TuRC (Oegema et al., 1999). To distinguish GCP4–GCP6 from the core components of the γ-TuSC, they are also called non-core components. After high-salt treatment, the γ-TuRC dissociates into the γ-TuSC (Oegema et al., 1999; Zhang et al., 2000). In most animal and plant cells, the non-core components of the γ-TuRC play essential roles in γ-tubulin-related MT organization (Kong et al., 2010; Murphy et al., 2001). In contrast, these components are not essential in *Drosophila melanogaster*, *Schizosaccharomyces pombe* and *A. nidulans* (Anders et al., 2006; Vérollet et al., 2006; Xiong and Oakley, 2009). In *A. nidulans*, any single deletion of the γ-TuRC-specific components GcpD, GcpE and GcpF and double and triple mutants are viable (Xiong and Oakley, 2009).

MTOCs are present in different forms in animals, plants and fungi. The prominent MTOC in higher eukaryotes is the centrosome and its functional ortholog in fungi are the SPBs. Different from what is seen in animal cells, plants lack centrosomes but employ an acentrosome system (Binarová et al., 2006; Murata et al., 2005; Stoppin et al., 1994). The simplest, but best characterized MTOC is the SPB of *S. cerevisiae*. It consists of a three-layered structure embedded into the nuclear envelope. The outer plaque of the SPB polymerizes cytoplasmic MTs in interphase and astral MTs during mitosis, while the inner plaque produces the mitotic spindles (Jaspersen and Winey, 2004). Both plaques share the γ-TuSC. However, both plaques apply different γ-tubulin complex receptors. Spc72 (named Mto1 in *S. pombe* and ApsB in *A. nidulans*) recruits the γ-tubulin complexes to the outer plaque, while Spc110 (named Pcp1 in *S. pombe* and PcpA in *A. nidulans*) recruits them to the inner plaque (Chen et al., 2012; Knop and Schiebel, 1997; Knop and Schiebel, 1998; Lin et al., 2015; Nguyen et al., 1998; Samejima et al., 2008, 2010; Soues and Adams, 1998).

[1]Karlsruhe Institute of Technology (KIT) - South Campus, Institute for Applied Biosciences, Dept. of Microbiology, Fritz-Haber-Weg 4, D-76131 Karlsruhe, Germany. [2]Tsukuba University, Faculty of Life and Environmental Sciences, Tsukuba 305-8572, Japan.

*Author for correspondence (reinhard.fischer@KIT.edu)

R.F., 0000-0002-6704-2569

Received 28 May 2019; Accepted 28 October 2019

Journal of Cell Science (2019) 132, jcs234799. doi:10.1242/jcs.234799

One interesting aspect of *A. nidulans*, in comparison to, for example, *S. cerevisiae*, is that two types of MTOCs have been described, SPBs and non-centrosomal septal MTOCs, and their structures and compositions appear to be different (Konzack et al., 2005; Zekert et al., 2010; Zhang et al., 2017). This situation is similar to *S. pombe* where two non-centrosomal MTOCs are found, the interphase (i)MTOCs and equatorial (e)MTOCs (Piel and Tran, 2009). However, in *S. pombe* those MTOCs are only transient structures, whereas sMTOCs of *A. nidulans* are formed during septation and remain at septa permanently (Heitz et al., 2001; Zhang et al., 2017). The SPBs in *A. nidulans* generate spindles and astral MTs during mitosis and cytoplasmic MTs during interphase (Manck et al., 2015; Morris and Enos, 1992; Suelmann et al., 1997). Several components of SPBs, like the γ-TuRC and the outer plaque receptors ApsB and Spa18 (Mto2 in *S. pombe* and absent in *S. cerevisiae*) are found at sMTOCs, while the inner plaque receptor PcpA (Pcp1 in *S. pombe* and Spc110 in *S. cereviase*) and proteins required for SPB duplication are missing at septa. As a further difference, an intrinsically disordered protein, Spa10, has been identified as an anchor of sMTOCs, and is targeted to septa earlier than ApsB or Spa18 and concentrated as a central disk structure at mature septa (Zhang et al., 2017). This protein is not present at SPBs. Moreover, *A. nidulans* has both large and small γ-tubulin complexes (Xiong and Oakley, 2009). However, it remained open to what extent the two complexes exist, or whether the small complexes are the result of a salt-dependent dissociation of GCPs from the γ-TuRC.

Recently, novel MTOC proteins were discovered in human and named mitotic-spindle organizing protein associated with a ring of γ-tubulin or short, MOZART proteins. Three isoforms were described, MOZART1, MOZART2A and MOZART2B (also known as MZT1, MZT2A and MZT2B, respectively) (Cota et al., 2017; Hutchins et al., 2010; Teixidó-Travesa et al., 2010). MOZART2A/2B, also both called GCP8, are involved in interphase MT organization. MOZART2A and 2B are only conserved in the deuterostome lineage, while MOZART1 is conserved in most eukaryotes including in *Xenopus laevis*, *D. melanogaster*, *Arabidopsis thaliana* [GIP1a,b or GIP2/GIP1 (Janski et al., 2012; Nakamura et al., 2012), *S. pombe* (Tam4/Mzt1; Dhani et al., 2013; Masuda et al., 2013)] and *Candida albicans* (CaMztA; Lin et al., 2016), but not in *S. cerevisiae*. MOZART1 is a novel component of the γ-TuRC. In *S. pombe*, Mzt1 is essential for MT nucleation and γ-TuRC recruitment to MTOCs (Dhani et al., 2013; Masuda et al., 2013). In *C. albicans*, MztA interacts with the receptor proteins Spc72 and Spc110 to turn the γ-TuSC into an active MT nucleation template (Lin et al., 2016). Hence, MTOCs in fungi appear to be unexpectedly variable and can consist of γ-TuSCs without MOZART1 (*S. cerevisiae*), γ-TuSC with MOZART1 (*C. albicans*) and γ-TuRC with MOZART1 (*S. pombe*). In *D. melanogaster* MOZART has also been characterized and also revealed heterogenity of different MTOCs (Tovey et al., 2018). In *A. nidulans*, it was reported that MztA is involved in the regulation of septation through suppressing the phosphatase ParA (Jiang et al., 2018). However, nothing is known about the function of MztA in MTOCs and MT polymerization. In this study, we show that the outer plaque of the SPB of *A. nidulans* consists of γ-TuSCs without MztA and the inner plaque of γ-TuRCs including MztA. The non-centrosomal septal MTOCs contain MztA in combination with components from the outer plaque of the SPBs. In addition, we present evidence that the number of γ-TuRCs in MTOCs during interphase is dynamic.

RESULTS

MztA localizes to SPBs and septal MTOCs in *A. nidulans*

We identified gene AN1361 in *A. nidulans* whose translation product showed high similarity to *H. sapiens* MOZART1 (56% identity),

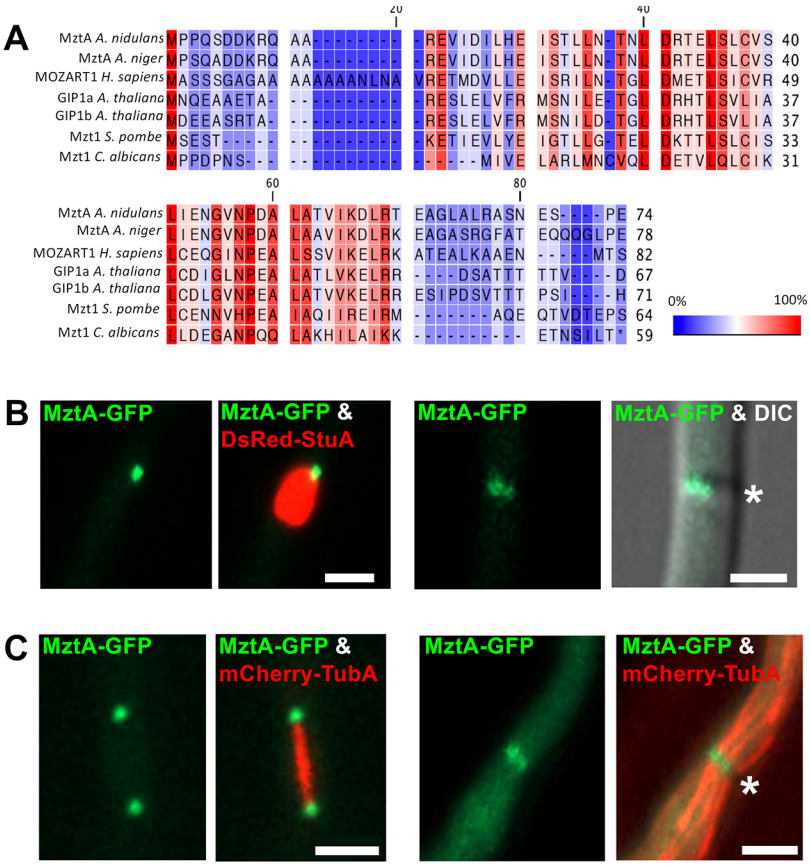

Fig. 1. Localization of the homolog of the MOZART1 protein, MztA, in *A. nidulans*. (A) Alignment of *A. nidulans* MztA and its orthologs in *Aspergillus niger* (Mzt1), *Arabidopsis thaliana* (GIP1a and GIP1b), *Homo sapiens* (MOZART1), *Schizosaccharomyces pombe* (Mzt1) and *Candida albicans* (CaMzt1). The alignment was performed with CLC Sequence Viewer 6.6.1 (Qiagen, Venlo, Netherlands) (gap open cost, 10.0; gap extension cost, 1.0). The background color indicates the conservation percentage as shown in the color bar. (B,C) Localization of MztA at SPBs and at sMTOCs *in vivo*. Strains SMS4 (*mztA::GFP*), SXL32 [*mztA::GFP; alcA(p)::DsRed::stuA(NLS)*] and SXL36 [*mztA::GFP; alcA(p)::mCherry::tubA*] were incubated in MM (2% glycerol with auxotrophic markers) at 28°C overnight. Nuclei, MztA, TubA were labelled with the fluorescent proteins indicated. Asterisks indicate the septum position. Scale bars: 2 µm.

Journal of Cell Science (2019) 132, jcs234799. doi:10.1242/jcs.234799

S. pombe Mzt1 (52%) and *C. albicans* Mzt1 (40%) (Fig. 1A). It had been previously been named *mztA* (Jiang et al., 2018). The gene is 379 bp in length and is located on chromosome VIII. In *S. pombe* Mzt1 was originally described as a 94-amino-acid-long protein, later corrected to being 64 amino acids long (Dhani et al., 2013; Hutchins et al., 2010; Masuda et al., 2013). In *A. nidulans* two versions were also predicted, of 64 and 74 amino acids in length. RNAseq data from our laboratory confirmed two introns (the ATG of the shorter version lies in the intron region), and re-complementation of a deletion mutant (see below) was only possible with the long version.

To characterize MztA in *A. nidulans*, we first asked whether MztA is a component of SPBs and septal MTOCs (Fig. 1B). All γ-TuRC components (γ-tubulin, GcpB, GcpC, GcpD, GcpE and GcpF) located to both types of MTOCs (Xiong and Oakley, 2009). Endogenous *mztA* was fused with GFP at its 3′ end and visualized in a strain where nuclei were labeled with DsRed (Toews et al., 2004). All nuclei showed one bright green spot, suggesting that MztA was a SPB-associated protein (data not shown). To co-visualize MztA and mitotic spindles, the MztA–GFP construct was transformed into a strain expressing mCherry-tagged α-tubulin. The green fluorescent signals clearly localized to the poles of the mitotic spindles (Fig. 1C, left panels). In addition to the SPB localization, MztA localized as several dots at septa, as was previously described for other sMTOC components (Zhang et al., 2017) (Fig. 1B,C, right panels). These localization patterns are reminiscent of the localization of GcpC or γ-tubulin. In order to exclude a possible interference of GFP with MztA function, we showed that the MztA–GFP construct fully rescued the *mztA* deletion phenotype (data not shown). By contrast, N-terminally tagged MztA only localized to SPBs but not to septa, indicating that the N-terminus is important for sMTOC recruitment (Fig. S1A). In order to prove the MztA localization with an alternative method, we tagged MztA C-terminally with the small HA tag and performed immunofluorescence analysis with the transgenic strains. MztA–HA clearly localized to SPBs (Fig. S1B), and also at septa (data not shown). Signals at septa were very weak. In addition, immunostaining always leads to some spot-like, unspecific signals in the cytoplasm, making it difficult to distinguish septal signals from those unspecific signals. We excluded the possibility of MztA locating at kinetochores, which also appear as a single spot at nuclei, by showing that MztA–GFP and mRFP–KatA did not colocalize (Fig. S1C).

MztA is dispensable for hyphal growth but is required for development

To gain insights into MztA functions, we deleted the entire open reading frame (ORF) of *mztA* by homologous recombination. The deletion event was confirmed by diagnostic PCR and southern blotting. In contrast to the case in *S. pombe*, *mztA* is not essential in *A. nidulans* (Dhani et al., 2013; Jiang et al., 2018; Masuda et al., 2013) (Fig. 2A–D). The sporulation of the Δ*mztA* strain was decreased as compared to wild type but not as much as in *apsB* deletion mutants. In *apsB* mutants, the primary defect is a nuclear migration defect due to reduced astral MT formation (Suelmann et al., 1998). Conidiophores of the *mztA* deletion strain, however, resembled wild-type conidiophores and nuclear migration appeared

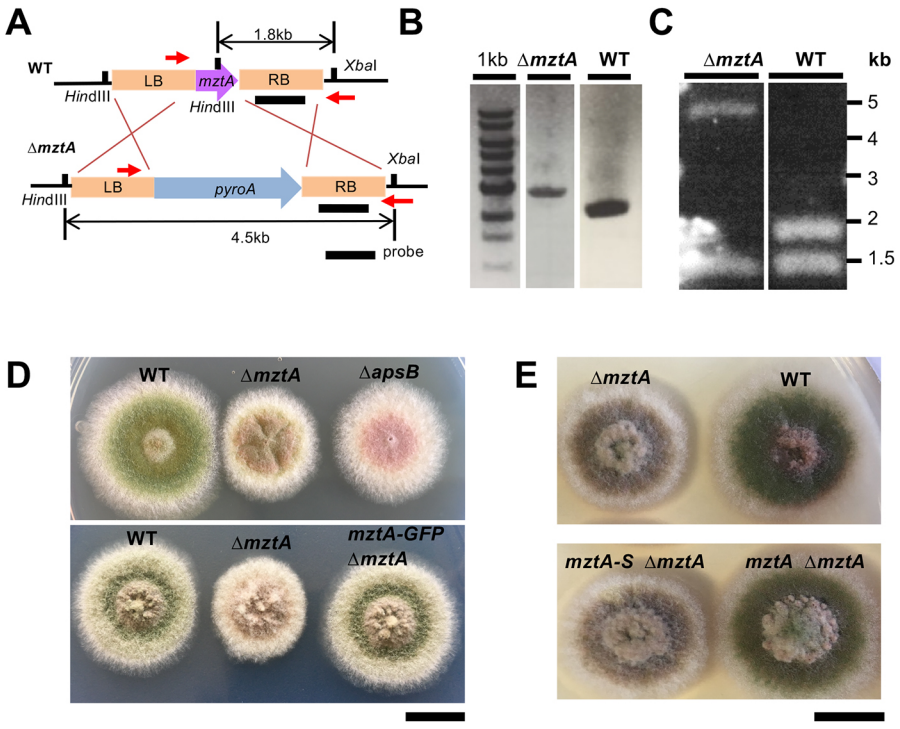

Fig. 2. Characterization of the *mztA* mutant. (A) Scheme of the deletion strategy. LB and RB represent the flanking regions of the *mztA* open reading frame. (B,C) Diagnostic PCR and Southern blot analysis of the *mztA* mutant strain. Primer pairs as indicated in B were used to prove homologous integration of the cassette. The Southern blot was used to exclude ectopic integrations of the construct. The right border (RB) was used as the probe in the Southern blotting. Whereas in wild type a 1.8 kb was detected, the band shifted to 4.5 kb in the mutant. In both, wild type (WT) and the Δ*mztA* mutant strain, a band at 1.5 kb was observed. This is due to cross-reaction with the probe. Lanes in B and C are from the same gel/blot, but non-relevant lanes are not shown. (D) Comparison of colonies of the following strains: wild type, the Δ*mztA*, the Δ*apsB* strain and the Δ*mztA*-strain re-complemented with the MztA–GFP construct. Strains SYZ3 (Δ*apsB*), SXL49 (Δ*mztA*), SXL144 (*mztA::GFP;* Δ*mztA*) and wild type (TN02A3) were grown on MM agar plates supplemented with corresponding supplements and 2% glucose for 3 days at 37°C. Scale bars: 1 cm. (E) Recomplementation of the *mztA* mutation with different *mztA* constructs. Strains TN02A3, SXL49 (Δ*mztA*), SXL103 (Δ*mztA; gpdA(p)::mztA379*), SXL104 (Δ*mztA; gpdA(p)::mztA255*) were grown on MM agar plates supplemented with appropriate supplements and 2% glucose for 3 days at 37°C. Scale bar: 1 cm.

Journal of Cell Science (2019) 132, jcs234799. doi:10.1242/jcs.234799

not to be affected (data not shown). The developmental phenotype was completely rescued after transformation with the wild-type *mztA* or the MztA–GFP construct (Fig. 2D). A putative shorter MztA variant (MztA-S) did not complement (Fig. 2E).

As a difference to what was seen in wild type, we observed more elongated nuclei in hyphae, suggesting a delay in mitosis. To test for a role for MztA in mitosis, we introduced GFP-tagged TubA into the Δ*mztA* strain and into wild type. Mitosis required ∼10 min in the *mztA* mutant and only ∼5 min in wild type (Fig. 3A,C). A total of 60% of the spindles in the Δ*mztA* strain showed abnormal morphologies (bent spindles, loose bipolar spindles and loose monopolar spindles; Fig. 3B,C). In wild type, defective spindles are very rare. Thus, MztA plays an important role in spindle assembly and stability, and reduced spore formation appears to be a consequence of retarded mitoses and not of astral MT malfunction.

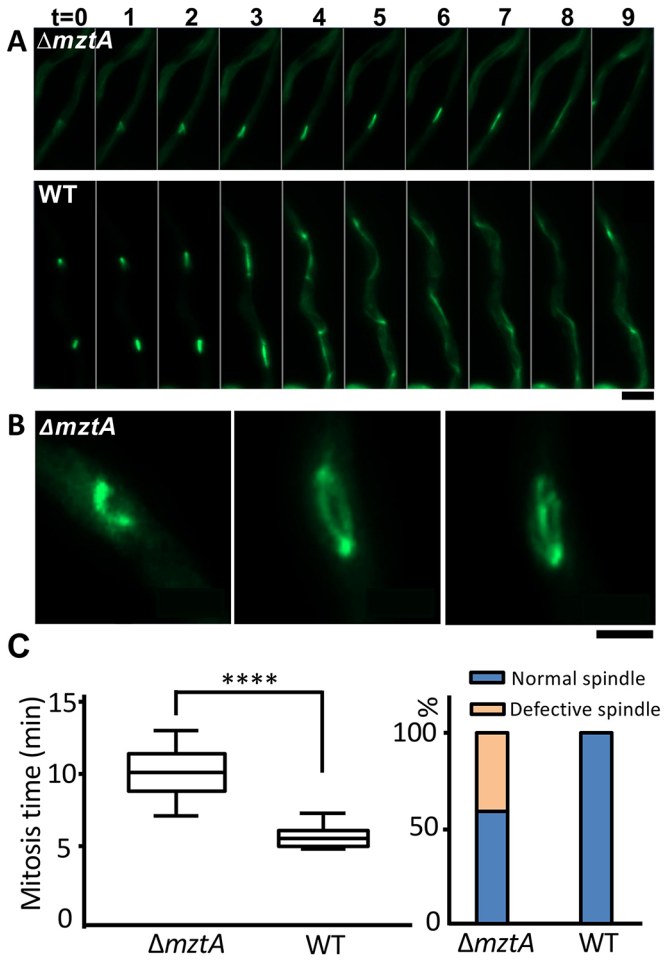

Fig. 3. The role of MztA during mitosis. (A) Comparison of mitosis in a Δ*mztA* mutant and wild type (WT). Strains SXL52 [Δ*mztA, alcA(p)::GFP::tubA*] and SJW02 [*alcA(p)::GFP::tubA*] were grown in eight-well u-slides at 28°C overnight for long-term live-cell observation. Time-lapse images were taken every 1 min at room temperature. In wild type, mitosis finished after 5 min while in the Δ*mztA* strain mitosis was prolonged. Scale bar: 5 µm. (B) Three types of unconventional spindles: bent, loose bipolar, and loose monopolar spindles. Strain SXL52 [Δ*mztA, alcA(p)::GFP::tubA*] was grown as above. Scale bar: 2 µm. (C) Quantification of the mitosis duration time and spindle states in a Δ*mztA* mutant and the wild-type strain. 20 events of mitosis were counted in each strain. Left panel, mitosis duration time. The box represents the 25–75th percentiles, and the median is indicated. The whiskers show the complete range. ****P<0.0001 (Mann–Whitney U-test). Right panel, 60% of the spindles in the Δ*mztA* strain showed abnormal shapes, while in wild type all 20 spindles were normal.

Because MztA appears to play an important role for the functioning of the MT cytoskeleton, we did initial experiments to test whether deletion of *mztA* affects MT stability. We did not observe differences in the sensitivity towards the MT-destabilizing drug benomyl in comparison to wild type (data not shown).

Recruitment of MztA to sMTOCs depends strictly on ApsB, Spa18 and Spa10

To investigate the exact time for recruitment of MztA during septum formation, we constructed a strain in which mCherry-tagged tropomyosin TpmA was introduced into a strain with GFP-tagged MztA. TpmA binds specifically to F-actin and localizes very early at the septation site and follows the constricting ring (Bergs et al., 2016). We did not observe any colocalization of MztA and TpmA even at nearly mature septa (Fig. 4A). Thus, the time of recruitment of MztA was similar to ApsB and Spa18, which only appear at mature septa (Zhang et al., 2017).

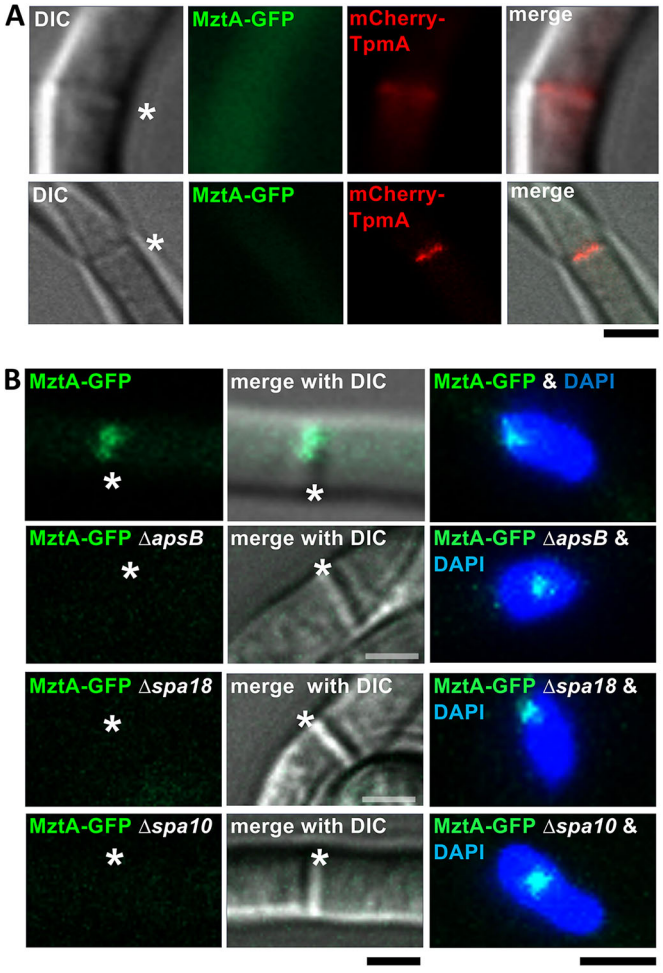

Fig. 4. Targeting MztA to sMTOCs depends on Spa10, ApsB and Spa18. (A) MztA is only targeted to mature septa. Analysis of the localization of MztA and TpmA in early and in nearly mature septa using fluorescent protein-tagged versions of MztA and TpmA. Strain SXL37 [*mztA::GFP; alcA(p)::mCherry::tpmA*] was incubated in MM (2% glycerol) at 28°C overnight. Scale bar: 2 µm. (B) Localization of MztA at sMTOC depends on Spa10, ApsB and Spa18. Strains SMS4 (*mztA::GFP*), SXL38 (Δ*apsB, mztA::GFP*), SXL39 (Δ*spa18, mztA::GFP*) and SXL42 (Δ*spa10, mztA::GFP*) were grown in MM with corresponding supplements at 28°C overnight. Nuclei were stained with DAPI. Asterisks indicate the septum position. Scale bars: 2 µm.

Journal of Cell Science (2019) 132, jcs234799. doi:10.1242/jcs.234799

Next, we asked whether MztA recruitment at septa requires ApsB and/or Spa18 (the orthologs of *S. pombe* Mto1 and Mto2) or the anchoring protein Spa10. MztA–GFP was introduced into *apsB*, *spa18* and *spa10* deletion mutants (Fig. 4B). MztA was not detected at septa in any of the gene deletion strains, while targeting to SPBs appeared to be unaffected. On the other hand, ApsB localization was not affected at SPBs nor at sMTOCs in the *mztA* deletion mutant (Fig. S2). These localization dependences are similar to that of the γ-TuRC component GcpC, which also requires Spa10, ApsB and Spa18 at sMTOCs (Zhang et al., 2017).

MztA interacts with GcpC and is essential for γ-TuRC recruitment to sMTOCs

Next, we tested whether MztA interacts with the γ-TuRC component GcpC. By using bimolecular fluorescence complementation (BiFC), we detected interaction of MztA and GcpC at SPBs (Fig. 5A, left upper panels). We confirmed this interaction via co-immunoprecipitation (co-IP) assays. In a strain containing MztA–GFP and 3HA–GcpC, we detected GcpC in the precipitate of MztA. In a strain containing only MztA–GFP or only 3HA–GcpC, no GcpC band was detected (Fig. 5A, lower panel). Thus, MztA binds directly to the γ-TuRC component GcpC. No interaction signal was detected at septa, indicating different arrangements of γ-TuRCs at nuclei and at septa (Fig. 5A, right upper panels).

We next asked whether MztA plays a role in GcpC recruitment to SPBs or to sMTOCs. We introduced GcpC–GFP into an *mztA* deletion strain and compared the GFP signal intensity to the one in a corresponding wild-type strain. At septa, GcpC signals were observed in wild type but not in the *mztA* deletion strain (Fig. 5B). Therefore, we analyzed the sMTOC activity by using the MT plus-end-tracking kinesin 7 motor protein KipA (Konzack et al., 2005). In wild type, KipA signals continuously emerged from septa whereas in the *mztA* mutant the sMTOCs were inactive (Movies 1 and 2). At SPBs, the GcpC signal was detected in the *mztA* deletion strain with ∼70% of the intensity of that in wild type (Fig. 5C). Hence, MztA appears to be essential for MT polymerization at sMTOCs but not at SPBs.

MztA is a component only of the inner plaque of SPBs

The function of MztA in *A. nidulans* appeared to be different to the essential function in *S. pombe* or *C. albicans* (Dhani et al., 2013; Lin et al., 2016; Masuda et al., 2013). The different phenotypes of an *mztA* and an *apsB* mutant in *A. nidulans* suggested that MztA plays a role in the organization of mitotic spindles but not in nuclear distribution, which requires proper astral MT organization and thus proper function

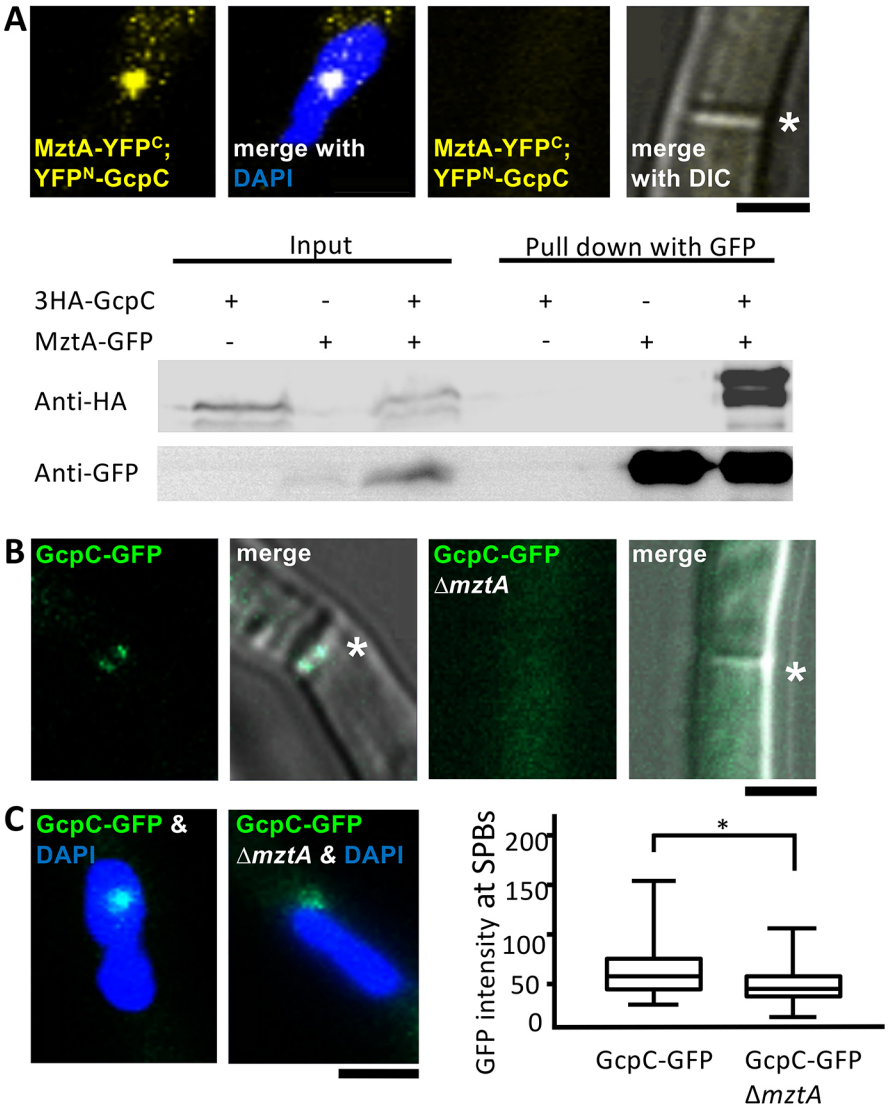

Fig. 5. Interaction analysis of MztA and GcpC and role of MztA in GcpC recruitment to sMTOCs and SPBs. (A) Interaction of MztA and GcpC as determined in bimolecular fluorescence complementation (BiFC, top) and co-IP (bottom) experiments. Top, strains SXL51 [*mztA::YFP^{C}; alcA(p)::YFP^{N}::gcpC*] and SXL78 (*mztA::YFP^{C}; gcpC::YFP^{N}*) were incubated in MM (2% glycerol) at 28°C overnight and imaged. Nuclei were stained with DAPI. Asterisks indicate the septum position. Scale bar: 2 µm. Bottom, co-IP between GcpC and MztA. Strain SXL108 [*alcA(p)::3HA::gcpC*; *mztA::GFP*] as well as control strains SMS4 (*mztA::GFP*) and SXL105 [*alcA(p)::3HA::gcpC*] were cultured in liquid MM containing 2% glycerol and 0.2% glucose plus required supplements for 24 h at 37°C. Co-IP was performed with anti-GFP agarose beads followed by SDS-PAGE and western blotting analysis. (B) *In vivo* analysis of the role of MztA for GcpC recruitment to sMTOCs. Strains SMS4 (*mztA::GFP*) and SXL53 (*ΔmztA::pyroA*; *gcpC::GFP*) were incubated in MM (2% glycerol) with supplements at 28°C overnight and imaged. Asterisks indicate the septum position. Scale bar: 2 µm. (C) Analysis of the role of MztA for GcpC recruitment to SPBs. The strains and inoculation conditions were the same as in A. Nuclei were stained with DAPI. Images of 10–15 sections were taken along the *z*-axis at 0.27 µm increments. Maximum projection images were obtained and maximum fluorescence intensities over the background were used for statistical analysis. The exposure time and shutter level were set to be identical. In total, 30 SPBs were checked in each strain. A quantification of the GFP intensity is shown in the graph. The box represents the 25–75th percentiles, and the median is indicated. The whiskers show the complete range. **P*<0.05 compared to wild type (Mann–Whitney *U*-test). Scale bar: 2 µm.

Journal of Cell Science (2019) 132, jcs234799. doi:10.1242/jcs.234799

of the outer plaque of the SPBs (Zhang et al., 2017). This prompted us to speculate that MztA locates and functions only at the inner plaque and not at the outer plaque of SPBs. To test this hypothesis, we assessed the colocalization of MztA with PcpA or ApsB. In a strain in which MztA was tagged with GFP and PcpA with mCherry, we found colocalization at nuclei in 82% of the observed SPBs (n=77) (Fig. 6A, upper panels). However, in a similar experiment with tagged MztA and ApsB, we observed a clear gap between the two fluorescent spots in 79% of the cases (n=63) (Fig. 6A, lower panels). The fact that in 21% of the observed SPBs, the MztA and ApsB signal overlapped is due to different observation angles (top view or side view). To further confirm this observation, we studied interaction of MztA with ApsB and/or PcpA. Indeed, there was interaction between MztA and PcpA as shown by BiFC, but not between MztA and ApsB as shown by BiFC and co-IP (Fig. 6B,C). Co-IP experiments with PcpA were unsuccessful, because PcpA was very unstable in our experiments. Taken together, we conclude that MztA resides only at the inner plaque of SPBs.

MztA recruits the γ-TuRC-specific component GcpD

A previous study revealed that the γ-TuRC-specific components GcpD, GcpE and GcpF are not essential for cell viability, spindle formation or sexual reproduction, and their localization at SPBs depends on the γ-TuSC (Xiong and Oakley, 2009). Here, we analyzed the localization of GcpD in the presence or absence of MztA. GcpD was tagged with mEosFP at the C-terminus. In wild type, GcpD–mEosFP dots were observed at nuclei. In the *mztA* deletion strain, the GcpD signal was completely absent. In comparison, GcpD SPB localization was independent of ApsB (Fig. S3A). To confirm that GcpD resides only at the inner plaque of SPBs, we did similar experiments to those for MztA. In a strain in which GcpD was tagged with GFP and PcpA fused with mCherry, we observed colocalization in 80% of SPBs (n=50). In contrast, GcpD and ApsB signals did not overlap at ∼80% of the nuclei (n=50) (Fig. S3B). We conclude that MztA recruits GcpD to the inner plaque of SPBs to assemble the γ-TuRC. Furthermore, this suggests that the outer plaque consists only of γ-TuSCs.

Stoichiometry and dynamics of MTOC proteins

To get more information on the organization of the different MTOCs in *A. nidulans*, we used photo-activated localization microscopy (PALM) to quantify the numbers of single molecules (Fig. 7A). In previous studies, the stoichiometry of MTOC components in yeast was determined biochemically (Masuda et al., 2013). However,

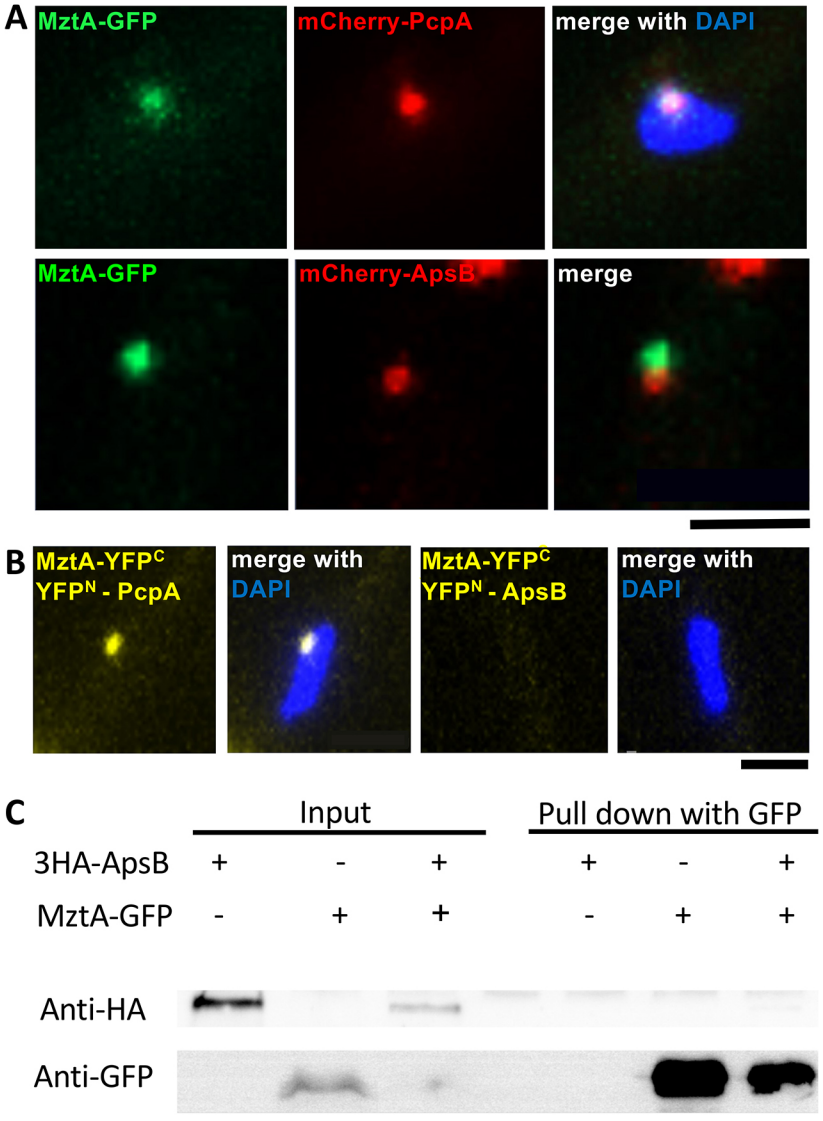

Fig. 6. Colocalization and interaction analysis of MztA with PcpA or ApsB. (A) Localization of MztA with PcpA or ApsB. Strains SXL88 [*mztA::GFP; alcA(p)::mCherry::apsB*] and SXL96 [*mztA::GFP; alcA(p)::mCherry::pcpA*] were incubated in MM (2% glycerol) at 28°C overnight and imaged. Nuclei were stained with DAPI. Scale bar: 2 µm. (B) Interaction analysis of MztA with PcpA or ApsB. Strains SXL82 [*mztA::YFP^{C}; alcA(p)::YFP^{N}::pcpA*] and SXL89 [*mztA::YFP^{C}; alcA(p)::YFP^{N}::apsB*] were incubated in MM (2% glycerol) at 28°C overnight and imaged. Nuclei were stained with DAPI. Scale bar: 2 µm. (C) Co-IP analysis confirmed that ApsB and MztA do not interact. Co-IP strains SXL109 [*alcA(p)::3HA::apsB*; *mztA::GFP*] as well as control strains SXL106 [*alcA(p)::3HA::apsB*] and SMS4 (*mztA::GFP*] were cultured in liquid MM containing 2% glycerol and 0.2% glucose with auxotrophic markers for 24 h at 37°C. Co-IP was performed with anti-GFP agarose beads followed by SDS-PAGE and western blot analysis.

Journal of Cell Science (2019) 132, jcs234799. doi:10.1242/jcs.234799

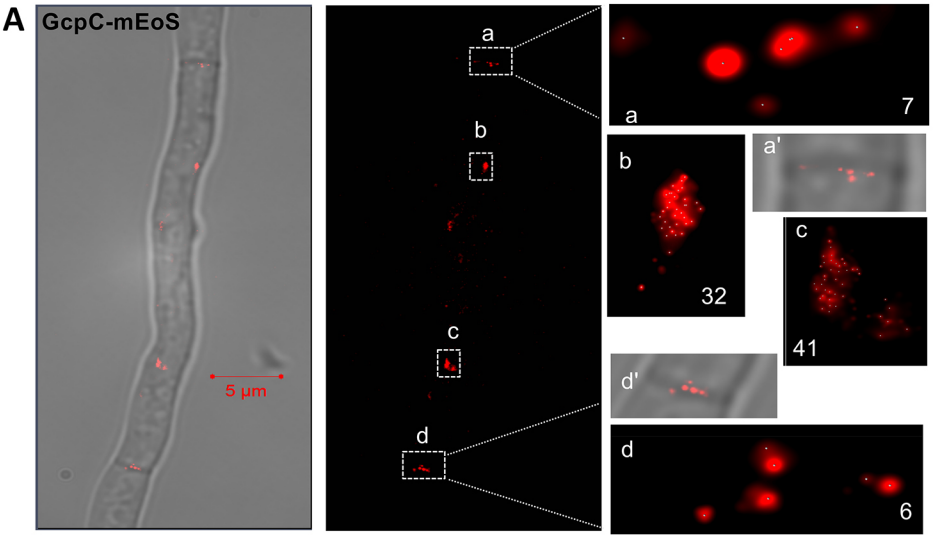

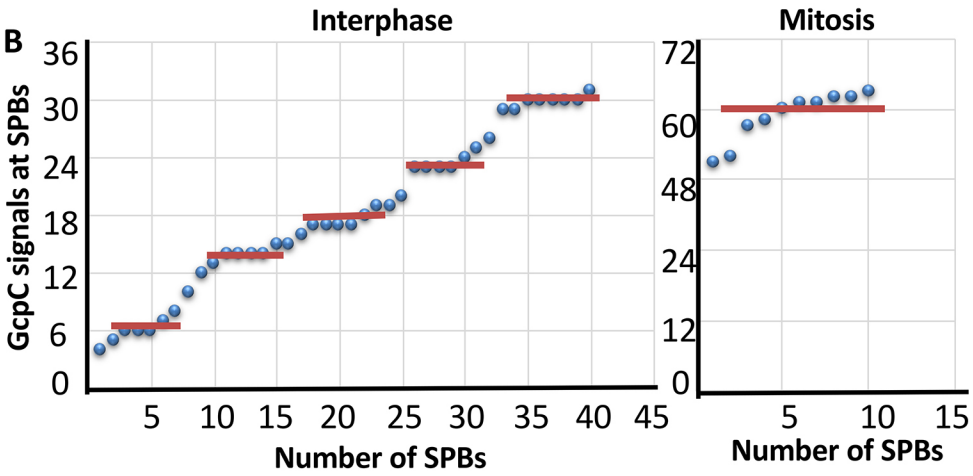

Fig. 7. Quantification of GcpC molecules by PALM super-resolution microscopy. (A) Representative images of GcpC–mEoS at two distinct SPBs and two sMTOCs in strain SXL98 (*gcpC::mEoS*). Areas b and c show signals counted from two SPBs. Areas a and d show signals from two sMTOCs. The right panels show enlarged images with the numbers of signals counted. Scale bar: 5 µm. (B) GcpC numbers are dynamic in interphase and stable in metaphase. A total of 40 SPBs in interphase and 10 SPBs during mitosis are included in the distribution analysis. The numbers of GcpC molecules per SPB were sorted ascendingly. The red line highlights discrete steps of GcpC numbers.

these methods did not allow SPBs and non-nuclear MTOCs to be distinguished in *A. nidulans*. We tagged the three γ-TuRC components GcpC, GcpD, and MztA, and the outer plaque receptor ApsB with mEoSFPthermo C-terminally and determined their numbers at SPBs and sMTOCs. The proteins were tagged at the native gene locus. We counted 22–60 SPBs and found ∼20 molecules of ApsB, ∼32 of GcpC, ∼10 of GcpD and ∼31 molecules of MztA at each interphase SPB (Table S4). The estimated molecular ratio of ApsB, GcpC, GcpD and MztA at SPBs in interphase was about 2:3:1:3 (Table S4). We also determined the number of proteins at sMTOCs. For each protein, 10–20 septa were analyzed. On average ∼5 molecules of GcpC, ∼3 molecules of GcpD and ∼6 molecules of MztA were found. Thus, the estimated molecular ratio of GcpC, GcpD and MztA at sMTOCs in interphase is about 3:2:4 (Table S4). We did not quantify ApsB at sMTOCs because C-terminal tagging of ApsB interfered with its localization. The molecular ratio of γ-TuRC at sMTOCs is different from that at SPBs, which might indicate a new structure of γ-TuRC assembly. We did not quantify ApsB at sMTOCs because C-terminal tagging of ApsB interfered with its localization.

Further interpretation of the molecular ratios of the analyzed proteins at SPBs appears to be difficult, because we noticed large fluctuations of the numbers of molecules during the cell cycle at individual SPBs. In the case of GcpC, numbers varied from 4 to 31 in interphase. When we plotted the numbers, we realized there were stepwise increases with multiples of 6 or 7 (Fig. 7B, left panel). Assuming that each γ-TuRC contains 13–14 γ-tubulin and 6–7 GcpC molecules, the number of γ-TuRCs ranges from 1 to 5. In addition, but rarely, GcpC numbers ranging up to 105 molecules were detected. The average increase of MTOC components from interphase to mitosis was between 50% and 100% (Table S4). The increase of MztA and GcpC numbers from interphase to mitosis was also obvious in intensity measurements undertaken with standard epifluorescence microscopy (data not shown). GcpC numbers (∼60) appeared to be constant during metaphase (Fig. 7B, right panel). With 5–6 GcpC molecules per γ-TuRCs, this number suggests the presence of ∼10 γ-TuRCs at each SPB during mitosis. The number of ApsB molecules at SPBs varied between 20 and 50 during mitosis (Fig. S4A). Assuming that each γ-TuSC contains between 14 and 20 ApsB molecules, as was calculated in *S. pombe* (Lynch et al., 2014), the number of γ-TuRCs would be between 1 and 3–4. This corresponds well to the small number of astral MTs polymerized from outer plaques. We also analyzed Spa18 at SPBs by time-lapse epifluorescence microscopy. At the beginning of mitosis, no Spa18 signals were detected at the very short mitotic spindles. As mitosis progressed, the signal intensity increased (Fig. S4B).

Journal of Cell Science (2019) 132, jcs234799. doi:10.1242/jcs.234799

DISCUSSION

The composition and functioning of MTOCs is a fascinating field of research, where the study of lower eukaryotes such as *S. cerevisiae* and *S. pombe* revealed many important insights (Cavanaugh and Jaspersen, 2017; Ruthnick and Schiebel, 2018; Wu and Akhmanova, 2017). Here, we studied *A. nidulans* protein MztA, the homolog of the MTOC protein MOZART1, relatively recently discovered in humans, and found that it is not required for viability but is required for development. We discovered that the SPB is composed of γ-TuSCs at the outer and γ-TuRCs at the inner plaque. MztA was only found at the inner plaque. The septal MTOCs also contain MztA, but the anchorage of the γ-TuRCs resembles the anchorage of the γ-TuSCs at the outer plaque of SPBs. Thus, sMTOCs combine properties of both, the outer and the inner plaque of SPBs (Fig. 8A). Our data add to the increasing complexity of MTOCs in eukaryotes, with different compositions, architectures and functions (Fig. 8A). Hence, in *S. cerevisiae*, *C. albicans*, *S. pombe* and *A. nidulans* four different γ-tubulin complexes are described, γ-TuSC, γ-TuSC with MOZART, γ-TuRC with MOZART and γ-TuRC with MOZART but alternative receptors (Cavanaugh and Jaspersen, 2017; Lin et al., 2016; Xiong and Oakley, 2009). *A. nidulans*, in addition offers the opportunity to study different MTOCs in a cell. This resembles the situation in other eukaryotes, such as *D. melanogaster*, where centrosomes and several non-centrosomal MTOCs have been described (Tillery et al., 2018; Tovey et al., 2018).

Our results will be discussed mainly as three points: (1) the role of MOZART in MTOC functioning, (2) the organization of the *A. nidulans* SPBs and sMTOCs, and (3) the dynamics of the composition of the SPB.

The role of MztA for recruiting γ-tubulin complexes and activating MT nucleation

In *S. pombe* and *C. albicans*, Mzt1 plays crucial roles for the recruitment of γ-TuSCs to SPBs and activation of MT nucleation (Dhani et al., 2013; Masuda et al., 2013). In *C. albicans*, Mzt1 together with the receptor proteins Spc110 and Spc72 promote γ-TuSC oligomerization into active MT nucleation rings (Lin et al., 2016). Hence, Mzt1 plays a dual role in *C. albicans* in the recruitment of γ-TuSCs to the SPBs and in their oligomerization and activation. However, in *A. nidulans*, the GcpC signal at SPBs was only reduced by 30% in the *mztA* mutant suggesting that MztA has lost the essential role for the recruitment of γ-TuSCs to SPBs. Still, it appears to improve the assembly. MztA has also lost its essential function for the activation of the γ-TuRC. Hence, the γ-TuRC of

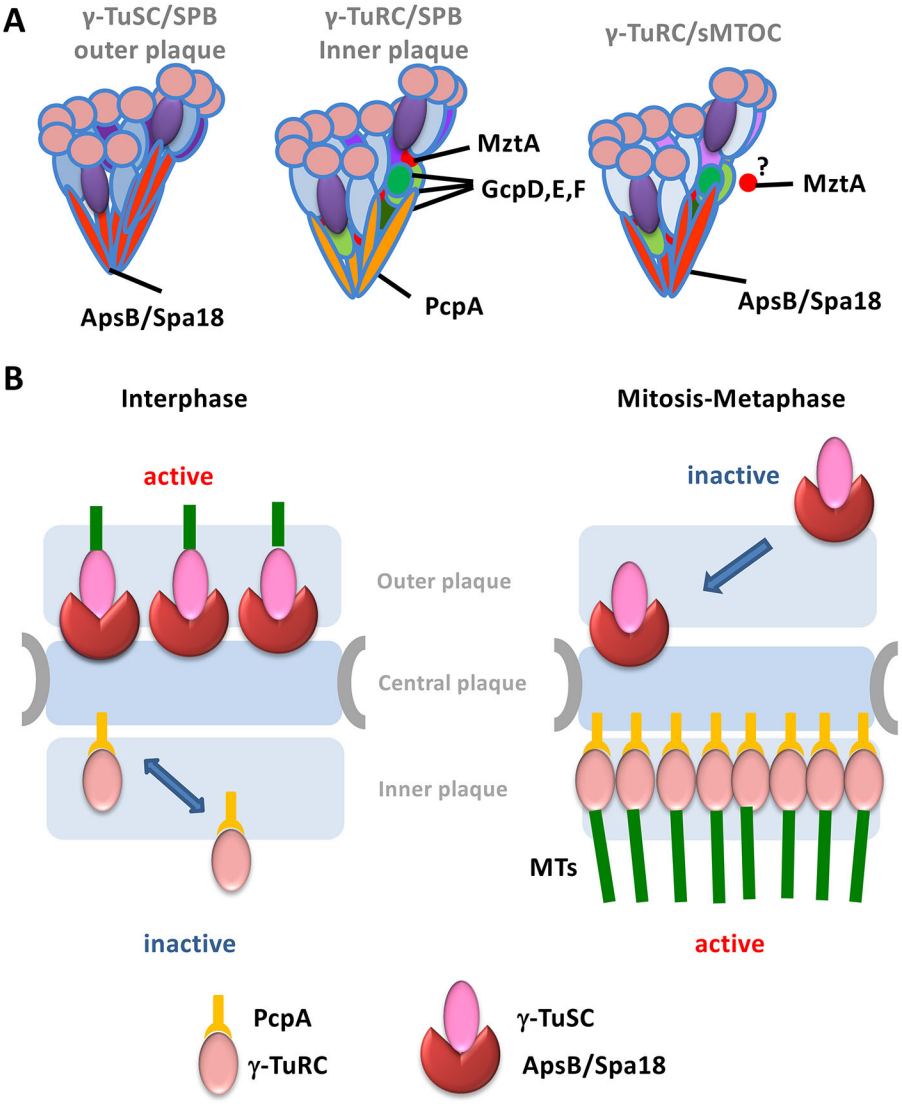

Fig. 8. Proposed model of MTOCs in *A. nidulans*. (A) In *A. nidulans* three types of γ-tubulin complexes are found. (1) γ-TuSCs without MztA. These are found at the outer plaque of SPBs and are anchored through ApsB and/or Spa18. (2) γ-TuRCs with MztA are found at the inner plaque of SPBs. They are anchored through PcpA. (3) γ-TuRCs with MztA at sMTOCs. These complexes are again anchored through ApsB and Spa18. The exact arrangement of the MztA protein in sMTOCs is not yet known. (B) Illustration of the dynamics of the SPB outer and inner plaque during interphase and during metaphase of mitosis.

Journal of Cell Science (2019) 132, jcs234799. doi:10.1242/jcs.234799

A. nidulans appears to be more similar to the γ-TuSC in *S. cerevisiae*, where MOZART is absent. However, MztA was essential for MTOC activity at septa. To explain this, it has to be considered that sMTOCs are comprised of γ-TuRCs, like the inner plaque of the *A. nidulans* SPB, but that the receptor proteins are the outer plaque proteins ApsB and Spa18. Taken together, we find that *A. nidulans* MztA plays an important role at the inner plaque of SPBs during mitosis and an essential role at sMTOCs during interphase. In human, the mitotic and the interphase functions of MOZART appear to be separated into two distinct proteins. Whereas MOZART1 (also called GCP9) is involved in γ-tubulin recruitment to centrosomes in mitotic cells, and its depletion leads to mitotic spindle defects (Hutchins et al., 2010), MOZART2 (also called GCP8) plays a role in γ-TuRC recruitment to interphase centrosomes (Teixidó-Travesa et al., 2010). Likewise, plant cells contain two homologous MOZART proteins, GIP1 and GIP2, or GIP1a and GIP1b. GIPs play roles in γ-tubulin complex localization and spindle stability during mitosis (Janski et al., 2012). Moreover, GIPs represent a subset of the *Arabidopsis* γ-tubulin complexes, which is consistent with the roles we have found for MztA (Nakamura et al., 2012). We therefore speculate that MztA in *A. nidulans* is more related to the proteins found in human or plant cells than in fission yeast, since MztA functions during mitosis as does MOZART1 in human or plant cells. The MOZART2 homolog, which should specifically function in interphase SPBs, is absent in *A. nidulans*. In contrast, Mzt1 in *S. pombe* or *C. albicans* combines the functions of MOZART1 and MOZART2. *A. nidulans* appears to be a link between γ-TuSCs functioning without the MOZART protein and fungi where MOZART is essential.

SPBs of *A. nidulans* are asymmetric and septal MTOCs are structurally different from SPBs

MztA specifically localizes at the inner plaque of *A. nidulans* SPBs and recruits γ-TuRC-specific components, whereas the outer plaque only contains γ-TuSCs (Fig. 8A). This asymmetric architecture is quite different from *S. cerevisiae* and *S. pombe*. In budding yeast, both plaques harbor only γ-TuSCs while in fission yeast both layers contain γ-TuRCs (Cavanaugh and Jaspersen, 2017). In *A. nidulans*, the outer plaque hence resembles the composition found in budding yeast, while the inner plaque resembles the composition found in fission yeast. The large γ-TuRC is composed of γ-tubulin, GcpB, GcpC, GcpD, GcpE, GcpF and MztA, and the latter four components are not essential for viability. A previous study described the hierarchy of the recruitment of the components with the order GcpF, GcpD and GcpE (Xiong and Oakley, 2009). Here, we showed that after γ-TuSC recruitment, MztA binds before GcpF, GcpD and GcpE.

The asymmetry of the SPB raises the question for reasons for this arrangement or the advantage of γ-TuRC being at the inner plaque in comparison to γ-TuSC. One explanation could be enhanced efficiency of MT nucleation during mitosis. However, we do not have evidence yet that the outer plaque of the SPB is less efficient in MT polymerization than sMTOCs, which contain γ-TuRCs and MztA. Another possibility could be that MztA might be involved in the regulation of spindle formation through interaction with specific kinases, such as the polo-like kinase PlkA. PlkA plays important roles in spindle assembly and corresponding mutants exhibit similar spindle defects to those seen in *mztA* mutants (Bachewich et al., 2005; Mogilevsky et al., 2012).

Thus, sMTOCs represent a novel class of γ-TuRC-containing MTOCs (Fig. 8A). The composition of sMTOCs is different from both the outer and the inner plaque of SPBs. sMTOCs consist of γ-TuRCs including MztA, GcpD, GcpE and GcpF, but also the outer plaque receptors ApsB and Spa18. In addition, a septal-pore associated protein Spa10 exclusively locates at sMTOCs (Zhang et al., 2017). The inner plaque receptor PcpA is missing in sMTOCs. The presence of MztA at the inner plaque and at sMTOCs may suggest some common regulation or coordination of the activities in a cell-cycle-dependent manner. However, the role of MztA appears to be different at sMTOCs and the inner plaque of SPBs. Whereas MztA is essential at sMTOCs, it is not in SPBs. Comparable to the situation in *A. nidulans*, γ-TuRC heterogeneity has been reported for *D. melanogaster* (Tovey, et al., 2018)

Dynamic numbers of γ-TuRCs at SPBs during the cell cycle

The SPB is a highly dynamic structure given that it divides prior to mitosis once during each cell cycle. Likewise, we found that the number of several γ-TuRC proteins increases during mitosis. This holds true for inner and for outer plaque proteins. However, more astonishing was the observation that the numbers of γ-TuRCs at different SPBs varied drastically during interphase. Our calculations suggest the presence of 1 to 5 γ-TuRCs. The increase of the number of GcpC molecules occurred in steps of ∼6 molecules. This suggests the addition of preassembled γ-TuRCs rather than an assembly at the inner plaque. We cannot exclude the second possibility completely, because it could be that the assembly is extremely quick once initiated. There was already some evidence for such dynamics. For example, ultrastructural analyses of SPB in *S. cerevisiae* had previously revealed different sizes of the structure, suggesting different protein compositions (Byers and Goetsch, 1974). Later studies analyzing the fluorescent intensity of RFP-labeled PcpA suggested that the γ-TuRC receptor protein Spc110 (PcpA) was also dynamic during the cell cycle (Viswanath et al., 2017; Yoder et al., 2003). The authors found that the fluorescent intensity increased at the G1/S border during the cell cycle, when the daughter SPB was generated. By using FRAP experiments, they also found that ∼50% of Spc110 is exchanged in the old SPB. However, in this paper, we present the first direct evidence for changing numbers of γ-TuRC during interphase of the cell cycle. This observation raises the question of whether there could be an advantage of such dynamic behavior as compared to there being a stable structure.

The number of GcpC molecules at SPBs during mitosis was more stable and reached ∼60. Assuming that each γ-TuRC contains 5–6 GcpC molecules, this result suggests that there are ∼10 γ-TuRCs at each SPB, enough to connect each of the eight chromosomes of *A. nidulans*. However, in an electron microscopy study the number of MTs in mitotic spindles was determined to be 35–50 (Oakley and Morris, 1983), suggesting some release of MTs from the SPBs after their polymerization. This is in agreement with studies in haploid yeast cells using electron micrographs and tomographic reconstructions (Byers and Goetsch, 1974; Viswanath et al., 2017). It was shown that, in metaphase, that there are 16 kinetochore MTs, one for each of its 16 chromosomes, and 3–4 interpolar MTs (Winey and O'Toole, 2001).

The numbers of the outer plaque proteins ApsB and Spa18 gradually increased during mitosis while in the beginning of mitosis, no Spa18 was detected. This confirms that the outer plaque is inactive before anaphase because in the absence of ApsB or Spa18 γ-TuSCs cannot be recruited (Fig. 8B). In comparison to the step-wise increase of the number of GcpC molecules at the inner plaque, the gradual increase of ApsB at the outer plaque suggests assembly of the complex at the outer plaque rather than addition of pre-assembled γ-TuSC.

MATERIALS AND METHODS

Strains, plasmids and culture conditions

Supplemented minimal medium (MM) and complete medium (YAG) for *A. nidulans* were prepared as previously described, and standard strain

Journal of Cell Science (2019) 132, jcs234799. doi:10.1242/jcs.234799

construction procedures were used (Hill and Käfer, 2001). Expression of tagged genes under the control of the *alcA*-promoter was regulated by the carbon source: repression on glucose, de-repression on glycerol (2%), and induction on threonine (2%) (Waring et al., 1989). A list of *A. nidulans* strains used in this study is given in Table S1. Standard laboratory *Escherichia coli* strains (Top 10 F′) were used. Plasmids are listed in Table S2.

Molecular techniques

Standard DNA transformation procedures were used for *A. nidulans* (Yelton et al., 1984) and *Escherichia coli* (Sambrook and Russel, 1999). For PCR experiments, standard protocols were applied using a Biometra Personal Cycler (Biometra, Göttingen, Germany) for the reaction cycles. Phusion polymerase was used. Denaturation was achieved at 98°C, annealing temperatures were chosen according to the corresponding DNA oligonucleotides, and the polymerization temperature was 72°C. DNA oligonucleotides used in this study are listed in Table S3. DNA sequencing was undertaken commercially (MWG Biotech, Ebersberg, Germany). Total DNA was extracted from *A. nidulans* according to Zekert et al. (2010). Southern hybridizations were performed according to the DIG Application Manual for Filter Hybridization (Roche Applied Science, Technical Resources, Roche Diagnostics GmbH, Mannheim, Germany). The first-strand cDNA synthesis was carried out with a SuperScript III Reverse Transcriptase kit (Invitrogen).

Construction of deletion strains and complementation

The *mztA* deletion strain was created by protoplast transformation and homologous integration of a fusion PCR-derived knockout cassette. The flanking regions of *mztA* were amplified by PCR with genomic DNA as template, and primers mztA-LB_fwd/mztA-LB-pyroA linker_rev (see Table S3) for the upstream region of *mztA* and mztA-RB-pyroA linker_fwd/mztA-RB_rev for the downstream region. *pyroA* was amplified with pyroA_fwd/pyroA_rev. Then the left border (LB), *pyroA* and right border (RB) were fused together by fusion PCR with nested primers mztA-LB-N_fwd and mztA-RB-N_rev. The construct was ligated to pJET1.2/blunt, yielding vector pFY2. After transformation of pFY2 to TN02A3 and selection by diagnostic PCR (Table S3 primers; mztA-dele_check_fwd/mztA-RB_rev) and Southern blotting, the *mztA* deletion strain SXL49 was selected (Fig. S2).

We constructed two plasmids to check whether the 64 amino acid or 74 amino acid form of MztA could re-complement the mutant phenotype. The whole expressing frame, including promoter, ORF and AfpyrG, was fused into pJET with NEBuilder HiFi DNA Assembly Master Mix (NEB) in one step. Here we describe the 74 amino acid version. The *gpdA* promoter was amplified using primers: gpdA builder_fwd/gpdA_rev; ORF of MztA was amplified using primers: mztA379_gpdA linker_fwd/mztA_pyrG linker_rev and pyrG was amplified using primers: pyrG_fwd/pyrG builder_rev. The three fragments were ligated to pJET1.2/blunt resulting in plasmid pXL69. After transformation into the *mztA* deletion strain SXL49, the re-complementation strain SXL103 showed 100% complementation of the phenotype.

C-terminal tagging of proteins with GFP or mEoSFPthermo expressed under the native promoter

We tagged MztA with GFP at the C-terminus and expressed it from the natural promoter. One kb from the 3′-end of the *mztA* gene was amplified with the primer pair MztA-C-termi_fwd/MztA-C-termi_GA linker_rev, and 1 kb of the terminator region of the gene was amplified with the primer pair MztA-RB-pyrG linker_fwd/MztA-RB_rev. The fragment of *GFP::pyrG* cassette was amplified from pFNO3 (Yang et al., 2004) using primers GA linker_fwd/pyrG overhang_rev. Subsequently, the three fragments were fused together by fusion PCR with nested primers MztA-C-termi-N_fwd/MztA-RB-N_rev (Table S3). The construct was ligated to pJET1.2/blunt, resulting in plasmid pXL23. The plasmid was transformed into TN02A3, and the strain SMS4 where the construct replaced the endogenous 3′-end of the gene, was checked with primers pyrG check fwd/MztA C-termi check rev. The strain expresses MztA-GFP from the natural promoter and MztA-GFP is the only source of MztA. The same strategy was used for C-terminal tagging of mEoSFPthermo for MztA, GcpC, GcpD, ApsB. The primers were the same as the GFP-tagging cassette (Table S3). The fragment of *mEoSFP::pyrG* cassette was amplified from pRM35. The resulting plasmids are pXL60 (*mztA::mEoSFP::pyrG*), pXL63 (*gcpD::mEoSFP::pyrG*), pXL89 (*gcpD::GFP::pyrG*), pXL64 (*apsB::mEoSFP::pyrG*) and pXL66 (*gcpC::mEoSFP::pyrG*) (Table S2). After transformation into the wild-type TN02A3 strain, strains SXL85, SXL98, SXL99 and SXL100 were constructed (Table S1).

To check GcpC localization in an *mztA* deletion strain, we crossed the two strains SXL49 (Δ*mztA*) and SNZ-SH80 (GcpC–GFP) (Todd et al., 2007). After screening with microscopy and diagnostic PCR (primers: pyrG check fwd/gcpC C-termi check rev), the recombinant strain SXL53 was selected.

Colocalization of two proteins tagged with GFP and mCherry

To investigate the timing of the recruitment of MztA at septa, colocalization with the actin ring marker TpmA (tropomyosin) was analyzed. TpmA was tagged with mCherry at the N-terminus in strains where MztA was C-terminally tagged with GFP. The plasmid pXL9 pCMB17apx-*mCherry-tmpA* was transformed into SMS4 (MztA–GFP) yielding strain SXL37. The homologous integration event for TpmA was confirmed with primers alcA check fwd/tpmA 1 kb Int check rev (Table S3).

To investigate colocalization of MztA and kinetochore protein KatA, KatA was tagged with mCherry at the N-terminus in the MztA–GFP-expressing strain SMS4. The plasmid pSH33 pMCB17apx-m*RFP-katA* was transformed into SMS4 resulting in strain SXL68.

To investigate the colocalization of MztA with PcpA or ApsB, the C-terminal tagging cassette of MztA in pXL23 was transformed into strain SXL80 or SXL7, where PcpA or ApsB was N-terminally fused with mCherry. The resulting strains were SXL96 and SXL88, respectively. Homologous integration events were checked with primers pyrG check fwd/MztA C-termi check rev (Table S3). The same method was used for determining the colocalization of GcpD with PcpA or ApsB. Plasmid pXL89, which contains the C-terminal GFP cassette of GcpD, was transformed into strain SXL80 or SXL7, yielding strains SXL149 and SXL148. Homologous integration events were checked with primers pyrG check fwd/GcpD C-termi check rev (Table S3).

Bimolecular fluorescence complementation assay

To analyze the interaction of MztA with GcpC, ApsB or PcpA, a bimolecular fluorescence complementation assay (BiFC or Split YFP) was performed. In these analyses, MztA was tagged with YFP^C at the C-terminus under the control of the natural promoter. The C-terminal YFP^C tagging cassette was constructed similar to the GFP-tagging cassette via fusion PCR. The same primers were used as for creating the GFP tagging cassette. *YFP^C::pyrG* cassette was amplified. After fusion, the construct was ligated to pJET1.2/blunt, resulting in plasmid pXL31. We also constructed an YFP^N tagging cassette in pJET1.2 pXL30 using the same strategy. For the analysis of the interaction of MztA and GcpC, 1 kb of the *gcpC* open reading frame was amplified with primers gcpC_AscI_fwd and gcpC_PacI_rev, cloned into pMCB17apx-*YFP^N* vector, which contained *YFP^N* instead of *GFP*, yielding pXL33. The C-terminal YFP^C tagging cassette of GcpC was constructed with the same strategy as for MztA. For primers, see Table S3. The resulting plasmid is pXL50. Then pXL31 and pXL33 were co-transformed into TN02A3. After screening, the strain SXL5,1 where MztA was C-terminally tagged with YFP^C and GcpC was N-terminally tagged with YFP^N, was examined for YFP signals. In addition, pXL31 and pXL50 were also co-transformed into TN02A3. Strain SXL78, where MztA and GcpC were C-terminally tagged with YFP^C and YFP^N, was examined for YFP signals. All the YFP strains were checked for homologous integration events by PCR.

For the analysis of the interaction of MztA and PcpA, 1 kb of the *pcpA* open reading frame was amplified with primers pcpA_AscI_fwd and pcpA_PacI_rev, and cloned into pMCB17apx-*YFP^N* vector, giving pXL58. Then pXL31 and pXL58 were co-transformed into TN02A3. After screening, the resulting strain SXL82 was examined for YFP signals. The strain was checked for homologous integration by PCR. For the analysis of the interaction of MztA and ApsB, plasmids pXL59 (full-length *apsB* in pMCB17apx-*YFP^N*) and pXL31 were co-transformed into TN02A3. After three rounds of screening, no transformant showed YFP signals, suggesting no interaction between ApsB and MztA.

Co-immunoprecipitation assay

To confirm the interaction results of the BIFC assay, we performed co-IP assays. We constructed the Co-IP strains SXL108 and SXL109, where GcpC or ApsB were tagged with triple HA at the N-terminus of the protein, while MztA was tagged with GFP C-terminally. The control strains are SXL106, SXL107 and SMS4, where only one tag (HA or GFP) was present. The corresponding plasmids for the strains are pXL71 and pXL72. The homologous integration events were checked by PCR (Table S3). The Co-IP and control strains were pulled down with anti-GFP agarose beads and tagged proteins detected with anti-HA antibodies. GFP-Trap agarose beads were from Chromotek. HA antibodies were produced in rabbit and were from Sigma-Aldrich (H6908).

Light and fluorescence microscopy

For live-cell imaging, fresh spores were inoculated in 0.5 ml MM (2% glycerol for *alcA* promoter induction) with appropriate selection markers on 18×18 mm coverslips (Roth, Karlsruhe). The samples were incubated at 28° C overnight, followed by 2 h incubation at room temperature before microscopy. VECTASHIELD Mounting Medium with DAPI (Vector Laboratories) was used for staining nuclei in cells. Light and fluorescence images were taken with the Zeiss Microscope AxioImager Z1 (Carl Zeiss, Jena, Germany) and the software ZEN pro 2012, using the Planapochromatic 63× or 100× oil immersion objective lens, and the Zeiss AxioCam MR camera. Image and video processing was undertaken with ZEN pro 2012, Adobe Photoshop or ImageJ (National Institutes of Health, MD, USA).

Alternatively, for *in vivo* time-lapse microscopy, cells were incubated in u-slide 8-well glass-bottom dishes from Ibidi (cells in focus) in 0.5 ml MM+2% glycerol and appropriate supplements, and an additional 2 ml of medium was added after overnight incubation. Movies were taken at appropriate intervals for time-lapse and maximum projections of a deconvolved *z*-stack images were used. For quantification of fluorescence intensity, images of 15–20 sections were taken along the *z*-axis at 0.27 µm increments. After deconvolution, projection images of maximum intensity were obtained, and maximum fluorescence intensities over the background intensity were used for statistical data analysis. A 5×5 pixel region of interest (ROI) was selected and two 20×20 pixel regions around the ROI were used for background subtraction.

All super-resolution cell images (PALM) were obtained with an inverted microscope (ELYRA 3D-PALM; Carl Zeiss AG) equipped with a high numerical aperture oil immersion objective (α-plan-Apochromat, 100×, numerical aperture, 1.46; Carl Zeiss AG), multiple excitation laser lines (405, 473, and 561 nm), an image splitter Optosplit (Cairn Research Ltd, Faversham, UK) and an electron-multiplying charge-coupled device (EMCCD) camera (iXon Ultra 897; Andor Technology, Ltd., Belfast, Northern Ireland). The fluorescent proteins were photo-activated by using low intensity 405 nm light and excited by 561 nm simultaneous illumination. After passing through the excitation dichroic, fluorescence emission was filtered by a 607/50 band-pass filter and recorded with a back-illuminated EMCCD camera (iXon Ultra 897; Andor Technology, Ltd.) at 50 ms/frame. All PALM images were constructed from 2000 images using Zen software (Carl Zeiss AG) with the PALM method and quantified with IMARIS 9 software (BITPLANE).

Statistical analysis

Significant differences were calculated with the two-tailed Mann–Whitney *U*-test with GraphPad 7. *P*-values are **P*<0.05; ***P*<0.01; ****P*<0.001 and ns, not significant.

Acknowledgements

We thank E. Wohlmann for excellent technical assistance.

Competing interests

The authors declare no competing or financial interests.

Author contributions

Conceptualization: R.F.; Investigation: X.G., M.S., Y.Z., S.F., N.T.; Data curation: X.G.; Writing - original draft: X.G.; Writing - review & editing: R.F.; Supervision: R.F.; Project administration: R.F.; Funding acquisition: R.F.

Funding

This work was supported by the German Science Foundation (Deutsche Forschungsgemeinschaft; DFG), grant number Fi459/20-1, and the Japanese Science and Technology Agency (JST) ERATO (grant number JPMJER1502). X.G. was a fellow of the Chinese Scholarship Council (CSC).

Supplementary information

Supplementary information available online at
http://jcs.biologists.org/lookup/doi/10.1242/jcs.234799.supplemental

References

Anders, A., Lourenço, P. C. C. and Sawin, K. E. (2006). Noncore components of the fission yeast gamma-tubulin complex. *Mol. Biol. Cell* **17**, 5075-5093. doi:10.1091/mbc.e05-11-1009

Bachewich, C., Masker, K. and Osmani, S. (2005). The polo-like kinase PLKA is required for initiation and progression through mitosis in the filamentous fungus *Aspergillus nidulans*. *Mol. Microbiol.* **55**, 572-587. doi:10.1111/j.1365-2958.2004.04404.x

Bergs, A., Ishitsuka, Y., Evangelinos, M., Nienhaus, G. U. and Takeshita, N. (2016). Dynamics of actin cables in polarized growth of the filamentous fungus *Aspergillus nidulans*. *Front. Microbiol.* **7**, 682. doi:10.3389/fmicb.2016.00682

Binarová, P., Cenklová, V., Procházková, J., Doskočilová, A., Volc, J., Vrlík, M. and Bögre, L. (2006). Gamma-tubulin is essential for acentrosomal microtubule nucleation and coordination of late mitotic events in Arabidopsis. *Plant Cell* **18**, 1199-1212. doi:10.1105/tpc.105.038364

Byers, B. and Goetsch, L. (1974). Duplication of spindle plaques and integration of the yeast cell cycle. *Cold Spring Harb. Symp. Quant. Biol.* **38**, 123-131. doi:10.1101/SQB.1974.038.01.016

Cavanaugh, A. M. and Jaspersen, S. L. (2017). Big lessons from little yeast: budding and fission yeast centrosome structure, duplication, and function. *Annu. Rev. Genet.* **51**, 361-383. doi:10.1146/annurev-genet-120116-024733

Chen, P., Gao, R., Chen, S., Pu, L., Li, P., Huang, Y. and Lu, L. (2012). A pericentrin-related protein homolog in *Aspergillus nidulans* plays important roles in nucleus positioning and cell polarity by affecting microtubule organization. *Eukaryot. Cell* **11**, 1520-1530. doi:10.1128/EC.00203-12

Colombié, N., Vérollet, C., Sampaio, P., Moisand, A., Sunkel, C., Bourbon, H.-M., Wright, M. and Raynaud-Messina, B. (2006). The Drosophila gamma-tubulin small complex subunit Dgrip84 is required for structural and functional integrity of the spindle apparatus. *Mol. Biol. Cell* **17**, 272-282. doi:10.1091/mbc.e05-08-0722

Cota, R. R., Teixido-Travesa, N., Ezquerra, A., Eibes, S., Lacasa, C., Roig, J. and Lüders, J. (2017). MZT1 regulates microtubule nucleation by linking gammaTuRC assembly to adapter-mediated targeting and activation. *J. Cell Sci.* **130**, 406-419. doi:10.1242/jcs.195321

Dhani, D. K., Goult, B. T., George, G. M., Rogerson, D. T., Bitton, D. A., Miller, C. J., Schwabe, J. W. R. and Tanaka, K. (2013). Mzt1/Tam4, a fission yeast MOZART1 homologue, is an essential component of the gamma-tubulin complex and directly interacts with GCP3^{Alp6}. *Mol. Biol. Cell* **24**, 3337-3349. doi:10.1091/mbc.e13-05-0253

Heitz, M. J., Petersen, J., Valovin, S. and Hagan, I. M. (2001). MTOC formation during mitotic exit in fission yeast. *J. Cell Sci.* **114**, 4521-4532.

Hill, T. W. and Käfer, E. (2001). Improved protocols for Aspergillus minimal medium: trace element and minimal medium salt stock solutions. *Fungal Genet. Newsletter* **48**, 20-21. doi:10.4148/1941-4765.1173

Horio, T. and Oakley, B. R. (2003). Expression of Arabidopsis gamma-tubulin in fission yeast reveals conserved and novel functions of gamma-tubulin. *Plant Physiol.* **133**, 1926-1934. doi:10.1104/pp.103.027367

Horio, T., Uzawa, S., Jung, M. K., Oakley, B. R., Tanaka, K. and Yanagida, M. (1991). The fission yeast g-tubulin is essential for mitosis and is localized at microtubule organizing centers. *J. Cell Sci.* **99**, 693-700.

Hutchins, J. R. A., Toyoda, Y., Hegemann, B., Poser, I., Heriche, J. K., Sykora, M. M., Augsburg, M., Hudecz, O., Buschhorn, B. A., Bulkescher, J. et al. (2010). Systematic analysis of human protein complexes identifies chromosome segregation proteins. *Science* **328**, 593-599. doi:10.1126/science.1181348

Janski, N., Masoud, K., Batzenschlager, M., Herzog, E., Evrard, J.-L., Houlné, G., Bourge, M., Chabouté, M.-E. and Schmit, A.-C. (2012). The GCP3-interacting proteins GIP1 and GIP2 are required for gamma-tubulin complex protein localization, spindle integrity, and chromosomal stability. *Plant Cell* **24**, 1171-1187. doi:10.1105/tpc.111.094904

Jaspersen, S. L. and Winey, M. (2004). The budding yeast spindle pole body: structure, duplication, and function. *Annu. Rev. Cell Dev. Biol.* **20**, 1-28. doi:10.1146/annurev.cellbio.20.022003.114106

Jiang, P., Zheng, S. and Lu, L. (2018). Mitotic-spindle organizing protein Mzta mediates septation signaling by suppressing the regulatory subunit of protein phosphatase 2A-ParA in *Aspergillus nidulans*. *Front. Microbiol.* **9**, 988. doi:10.3389/fmicb.2018.00988

Julian, M., Tollon, Y., Lajoie-Mazenc, I., Moisand, A., Mazarguil, H., Puget, A. and Wright, M. (1993). gamma-Tubulin participates in the formation of the midbody during cytokinesis in mammalian cells. *J. Cell Sci.* **105**, 145-156.
Knop, M. and Schiebel, E. (1997). Spc98p and Spc97p of the yeast gamma-tubulin complex mediate binding to the spindle pole body via their interaction with Spc110p. *EMBO J.* **16**, 6985-6995. doi:10.1093/emboj/16.23.6985
Knop, M. and Schiebel, E. (1998). Receptors determine the cellular localization of a gamma-tubulin complex and thereby the site of microtubule formation. *EMBO J.* **17**, 3952-3967. doi:10.1093/emboj/17.14.3952
Kollman, J. M., Polka, J. K., Zelter, A., Davis, T. N. and Agard, D. A. (2010). Microtubule nucleating gamma-TuSC assembles structures with 13-fold microtubule-like symmetry. *Nature* **466**, 879-882. doi:10.1038/nature09207
Kong, Z., Hotta, T., Lee, Y.-R. J., Horio, T. and Liu, B. (2010). The gamma-tubulin complex protein GCP4 is required for organizing functional microtubule arrays in *Arabidopsis thaliana*. *Plant Cell* **22**, 191-204. doi:10.1105/tpc.109.071191
Konzack, S., Rischitor, P. E., Enke, C. and Fischer, R. (2005). The role of the kinesin motor KipA in microtubule organization and polarized growth of *Aspergillus nidulans*. *Mol. Biol. Cell* **16**, 497-506. doi:10.1091/mbc.e04-02-0083
Lin, T.-C., Neuner, A. and Schiebel, E. (2015). Targeting of gamma-tubulin complexes to microtubule organizing centers: conservation and divergence. *Trends Cell Biol.* **25**, 296-307. doi:10.1016/j.tcb.2014.12.002
Lin, T.-C., Neuner, A., Flemming, D., Liu, P., Chinen, T., Jäkle, U., Arkowitz, R. and Schiebel, E. (2016). MOZART1 and gamma-tubulin complex receptors are both required to turn gamma-TuSC into an active microtubule nucleation template. *J. Cell Biol.* **215**, 823-840. doi:10.1083/jcb.201606092
Liu, B., Joshi, H. C., Wilson, T. J., Silflow, C. D., Palevitz, B. A. and Snustad, D. P. (1994). gamma-Tubulin in Arabidopsis: gene sequence, immunoblot, and immunofluorescence studies. *Plant Cell* **6**, 303-314. doi:10.1105/tpc.6.2.303
Lynch, E. M., Groocock, L. M., Borek, W. E. and Sawin, K. E. (2014). Activation of the gamma-tubulin complex by the Mto1/2 complex. *Curr. Biol.* **24**, 896-903. doi:10.1016/j.cub.2014.03.006
Manck, R., Ishitsuka, Y., Herrero, S., Takeshita, N., Nienhaus, G. U. and Fischer, R. (2015). Genetic evidence for a microtubule-capture mechanism during polarised growth of *Aspergillus nidulans*. *J. Cell Sci.* **128**, 3569-3582. doi:10.1242/jcs.169094
Martin, O. C., Gunawardane, R. N., Iwamatsu, A. and Zheng, Y. (1998). Xgrip109: a gamma tubulin-associated protein with an essential role in gamma tubulin ring complex (gammaTuRC) assembly and centrosome function. *J. Cell Biol.* **141**, 675-687. doi:10.1083/jcb.141.3.675
Masuda, H., Mori, R., Yukawa, M. and Toda, T. (2013). Fission yeast MOZART1/Mzt1 is an essential gamma-tubulin complex component required for complex recruitment to the microtubule organizing center, but not its assembly. *Mol. Biol. Cell* **24**, 2894-2906. doi:10.1091/mbc.e13-05-0235
Mogilevsky, K., Glory, A. and Bachewich, C. (2012). The polo-like kinase PLKA in *Aspergillus nidulans* is not essential but plays important roles during vegetative growth and development. *Eukaryot. Cell* **11**, 194-205. doi:10.1128/EC.05130-11
Moritz, M., Braunfeld, M. B., Guénebaut, V., Heuser, J. and Agard, D. A. (2000). Structure of the gamma-tubulin ring complex: a template for microtubule nucleation. *Nat. Cell Biol.* **2**, 365-370. doi:10.1038/35014058
Morris, N. R. and Enos, A. P. (1992). Mitotic gold in a mold: *Aspergillus* genetics and the biology of mitosis. *Trends Genet.* **8**, 32-33. doi:10.1016/0168-9525(92)90022-V
Murata, T., Sonobe, S., Baskin, T. I., Hyodo, S., Hasezawa, S., Nagata, T., Horio, T. and Hasebe, M. (2005). Microtubule-dependent microtubule nucleation based on recruitment of gamma-tubulin in higher plants. *Nat. Cell Biol.* **7**, 961-968. doi:10.1038/ncb1306
Murphy, S. M., Preble, A. M., Patel, U. K., O'Connell, K. L., Dias, D. P., Moritz, M., Agard, D., Stults, J. T. and Stearns, T. (2001). GCP5 and GCP6: two new members of the human gamma-tubulin complex. *Mol. Biol. Cell* **12**, 3340-3352. doi:10.1091/mbc.12.11.3340
Nakamura, M., Yagi, N., Kato, T., Fujita, S., Kawashima, N., Ehrhardt, D. W. and Hashimoto, T. (2012). Arabidopsis GCP3-interacting protein 1/MOZART 1 is an integral component of the gamma-tubulin-containing microtubule nucleating complex. *Plant J.* **71**, 216-225. doi:10.1111/j.1365-313X.2012.04988.x
Nguyen, T., Vinh, D. B. N., Crawford, D. K. and Davis, T. N. (1998). A genetic analysis of interactions with Spc110p reveals distinct functions of Spc97p and Spc98p, components of the yeast gamma-tubulin complex. *Mol. Biol. Cell* **9**, 2201-2216. doi:10.1091/mbc.9.8.2201
Oakley, B. R. (2004). Tubulins in *Aspergillus nidulans*. *Fungal Genet. Biol.* **41**, 420-427. doi:10.1016/j.fgb.2003.11.013
Oakley, B. R. and Morris, N. R. (1983). A mutation in *Aspergillus nidulans* that blocks the transition from interphase to prophase. *J. Cell Biol.* **96**, 1155-1158. doi:10.1083/jcb.96.4.1155
Oakley, C. E. and Oakley, B. R. (1989). Identification of gamma-tubulin, a new member of the tubulin superfamily encoded by *mipA* gene of *Aspergillus nidulans*. *Nature* **338**, 662-664. doi:10.1038/338662a0
Oakley, B. R., Paolillo, V. and Zheng, Y. (2015). gamma-Tubulin complexes in microtubule nucleation and beyond. *Mol. Biol. Cell* **26**, 2957-2962. doi:10.1091/mbc.E14-11-1514
Oegema, K., Wiese, C., Martin, O. C., Milligan, R. A., Iwamatsu, A., Mitchison, T. J. and Zheng, Y. (1999). Characterization of two related Drosophila gamma-tubulin complexes that differ in their ability to nucleate microtubules. *J. Cell Biol.* **144**, 721-733. doi:10.1083/jcb.144.4.721
Piel, M. and Tran, P. T. (2009). Cell shape and cell division in fission yeast. *Curr. Biol.* **19**, R823-R827. doi:10.1016/j.cub.2009.08.012
Ruthnick, D. and Schiebel, E. (2018). Duplication and nuclear envelope insertion of the yeast microtubule organizing centre, the spindle pole body. *Cells* **7**, 42. doi:10.3390/cells7050042
Sambrook, J. and Russel, D. W. (1999). Molecular Cloning: A laboratory manual. *Cold Spring Harbor*, New York: Cold Spring Harbor Laboratory Press.
Samejima, I., Miller, V. J., Groocock, L. M. and Sawin, K. E. (2008). Two distinct regions of Mto1 are required for normal microtubule nucleation and efficient association with the gamma-tubulin complex *in vivo*. *J. Cell Sci.* **121**, 3971-3980. doi:10.1242/jcs.038414
Samejima, I., Miller, V. J., Rincon, S. A. and Sawin, K. E. (2010). Fission yeast Mto1 regulates diversity of cytoplasmic microtubule organizing centers. *Curr. Biol.* **20**, 1959-1965. doi:10.1016/j.cub.2010.10.006
Soues, S. and Adams, I. R. (1998). SPC72: a spindle pole component required for spindle orientation in the yeast *Saccharomyces cerevisiae*. *J. Cell Sci.* **111**, 2809-2818.
Stoppin, V., Vantard, M., Schmit, A.-C. and Lambert, A.-M. (1994). Isolated plant nuclei nucleate microtubule assembly: the nuclear surface in higher plants has centrosome-like activity. *Plant Cell* **6**, 1099-1106. doi:10.2307/3869888
Suelmann, R., Sievers, N. and Fischer, R. (1997). Nuclear traffic in fungal hyphae: *In vivo* study of nuclear migration and positioning in *Aspergillus nidulans*. *Mol. Microbiol.* **25**, 757-769. doi:10.1046/j.1365-2958.1997.5131873.x
Suelmann, R., Sievers, N., Galetzka, D., Robertson, L., Timberlake, W. E. and Fischer, R. (1998). Increased nuclear traffic chaos in hyphae of *Aspergillus nidulans:* Molecular characterization of *apsB* and *in vivo* observation of nuclear behaviour. *Mol. Microbiol.* **30**, 831-842. doi:10.1046/j.1365-2958.1998.01115.x
Teixidó-Travesa, N., Villén, J., Lacasa, C., Bertran, M. T., Archinti, M., Gygi, S. P., Caelles, C., Roig, J. and Lüders, J. (2010). The gammaTuRC revisited: a comparative analysis of interphase and mitotic human gammaTuRC redefines the set of core components and identifies the novel subunit GCP8. *Mol. Biol. Cell* **21**, 3963-3972. doi:10.1091/mbc.e10-05-0408
Tillery, M. M. L., Blake-Hedges, C., Zheng, Y., Buchwalter, R. A. and Megraw, T. L. (2018). Centrosomal and non-centrosomal microtubule-organizing centers (MTOCs) in *Drosophila melanogaster*. *Cells* **7**, 121. doi:10.3390/cells7090121
Todd, R. B., Davis, M. A. and Hynes, M. J. (2007). Genetic manipulation of *Aspergillus nidulans*: meiotic progeny for genetic analysis and strain construction. *Nat. Protoc.* **2**, 811-821. doi:10.1038/nprot.2007.112
Toews, M. W., Warmbold, J., Konzack, S., Rischitor, P., Veith, D., Vienken, K., Vinuesa, C., Wei, H. and Fischer, R. (2004). Establishment of mRFP1 as a fluorescent marker in *Aspergillus nidulans* and construction of expression vectors for high-throughput protein tagging using recombination in vitro (GATEWAY). *Curr. Genet.* **45**, 383-389. doi:10.1007/s00294-004-0495-7
Tovey, C. A., Tubman, C. E., Hamrud, E., Zhu, Z., Dyas, A. E., Butterfield, A. N., Fyfe, A., Johnson, E. and Conduit, P. T. (2018). gamma-TuRC heterogeneity revealed by analysis of Mozart1. *Curr. Biol.* **28**, 2314-2323. doi:10.1016/j.cub.2018.05.044
Vardy, L. and Toda, T. (2000). The fission yeast gamma-tubulin complex is required in G1 phase and is a component of the spindle assembly checkpoint. *EMBO J.* **19**, 6098-6111. doi:10.1093/emboj/19.22.6098
Vérollet, C., Colombié, N., Daubon, T., Bourbon, H.-M., Wright, M. and Raynaud-Messina, B. (2006). Drosophila melanogaster gamma-TuRC is dispensable for targeting gamma-tubulin to the centrosome and microtubule nucleation. *J. Cell Biol.* **172**, 517-528. doi:10.1083/jcb.200511071
Viswanath, S., Bonomi, M., Kim, S. J., Klenchin, V. A., Taylor, K. C., Yabut, K. C., Umbreit, N. T., Van Epps, H. A., Meehl, J., Jones, M. H. et al. (2017). The molecular architecture of the yeast spindle pole body core determined by Bayesian integrative modeling. *Mol. Biol. Cell* **28**, 3298-3314. doi:10.1091/mbc.e17-06-0397
Waring, R. B., May, G. S. and Morris, N. R. (1989). Characterization of an inducible expression system in Aspergillus nidulans using alcA and tubulin coding genes. *Gene* **79**, 119-130. doi:10.1016/0378-1119(89)90097-8
Winey, M. and O'Toole, E. T. (2001). The spindle cycle in budding yeast. *Nat. Cell Biol.* **3**, E23-E27. doi:10.1038/35050663
Wu, J. and Akhmanova, A. (2017). Microtubule-organizing centers. *Annu. Rev. Cell Dev. Biol.* **33**, 51-75. doi:10.1146/annurev-cellbio-100616-060615
Xiong, Y. and Oakley, B. R. (2009). *In vivo* analysis of the functions of gamma-tubulin-complex proteins. *J. Cell Sci.* **122**, 4218-4227. doi:10.1242/jcs.059196
Yang, L., Ukil, L., Osmani, A., Nahm, F., Davies, J., De Souza, C. P. C., Dou, X., Perez-Balguer, A. and Osmani, S. A. (2004). Rapid production of gene replacement constructs and generation of a green fluorescent protein-tagged centromeric marker in Aspergillus nidulans. *Eukaryot. Cell* **3**, 1359-1362. doi:10.1128/ec.3.5.1359-1362.2004

Yelton, M. M., Hamer, J. E. and Timberlake, W. E. (1984). Transformation of *Aspergillus nidulans* by using a *trpC* plasmid. *Proc. Natl. Acad. Sci. USA* **81**, 1470-1474. doi:10.1073/pnas.81.5.1470

Yoder, T. J., Pearson, C. G., Bloom, K. and Davis, T. N. (2003). The *Saccharomyces cerevisiae* spindle pole body is a dynamic structure. *Mol. Biol. Cell* **14**, 3494-3505. doi:10.1091/mbc.e02-10-0655

Zekert, N., Veith, D. and Fischer, R. (2010). Interaction of the *Aspergillus nidulans* mircrotubule-organizing center (MTOC) component ApsB with gamma-tubulin and evidence for a role of a subclass of peroxisomes in the formation of septal MTOCs. *Eukaryot. Cell* **9**, 795-805. doi:10.1128/EC.00058-10

Zhang, L., Keating, T. J., Wilde, A., Borisy, G. G. and Zheng, Y. (2000). The role of Xgrip210 in gamma-tubulin ring complex assembly and centrosome recruitment. *J. Cell Biol.* **151**, 1525-1536. doi:10.1083/jcb.151.7.1525

Zhang, Y., Gao, X., Manck, R., Schmid, M., Osmani, A. H., Osmani, S. A., Takeshita, N. and Fischer, R. (2017). Microtubule-organizing centers of *Aspergillus nidulans* are anchored at septa by a disordered protein. *Mol. Microbiol.* **106**, 285-303. doi:10.1111/mmi.13763

Zheng, Y., Wong, M. L., Alberts, B. and Mitchison, T. (1995). Nucleation of microtubule assembly by a gamma-tubulin-containing ring complex. *Nature* **378**, 578-583. doi:10.1038/378578a0

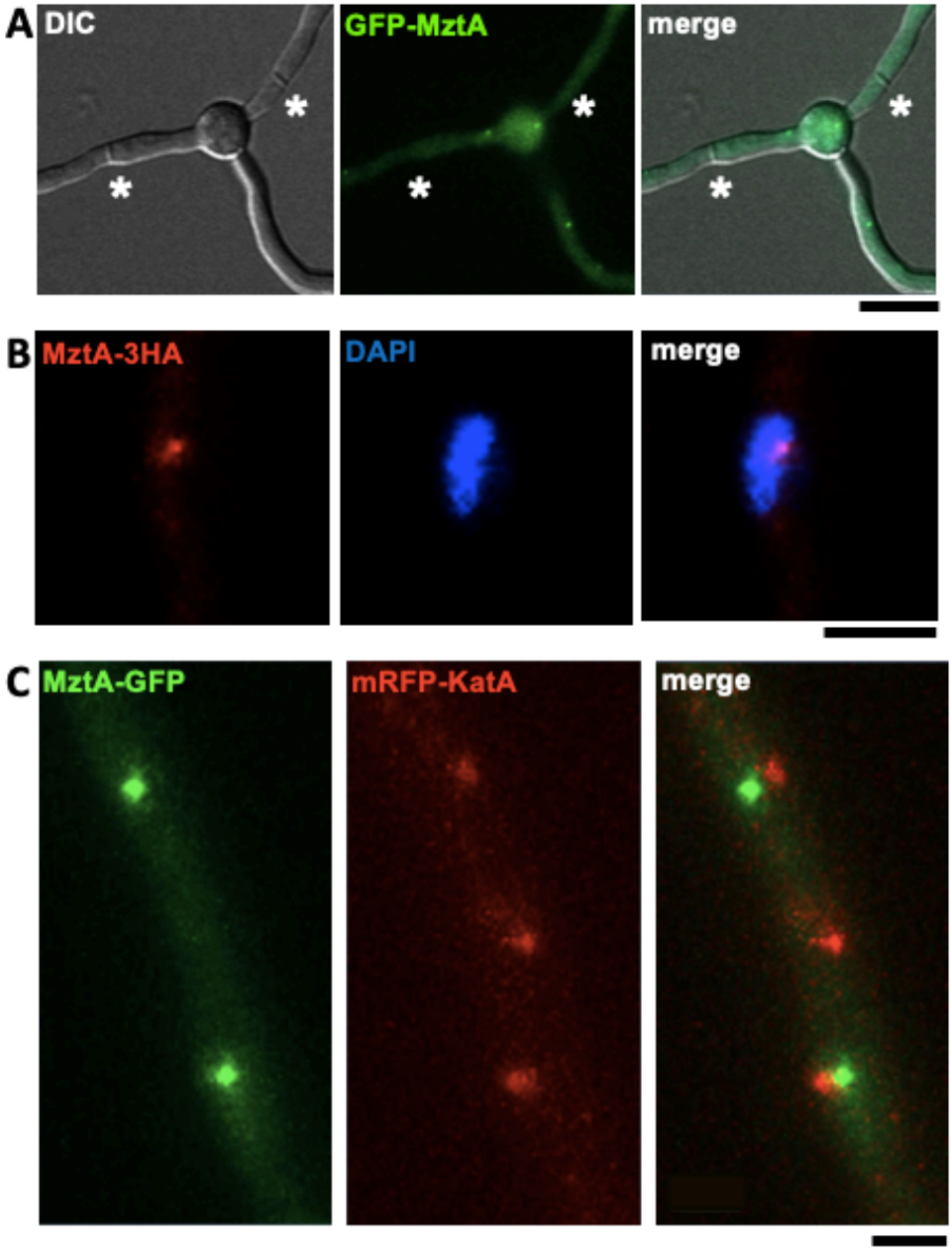

Fig. S1: Analysis of MztA localization using different tagging strategy. (A) GFP fusion at the N-terminus of MztA interrupted the septal localization. Strain SXL142 (*alcA(p)::GFP::mztA*) was incubated in MM (2% glycerol) with supplements at 28°C overnight. Asterisks indicate the septa positions. Scale bar, 2 µm. **(B)** Immunofluorescence images of MztA tagged with 3HA at its C-terminus. Strain SXL143 (*mztA::3HA*) was performed with anti-HA mouse 1st antibody and cys3 2nd antibody against mouse. Nuclei was stained with DAPI. **(C)** Localization of MztA compared to the kinetochore marker. Strain SXL68 (*alcA(p)::mRFP::katA*; *mztA::GFP*) was incubated in MM (2% glycerol) at 28°C overnight and imaged. Scale bar, 2 µm.

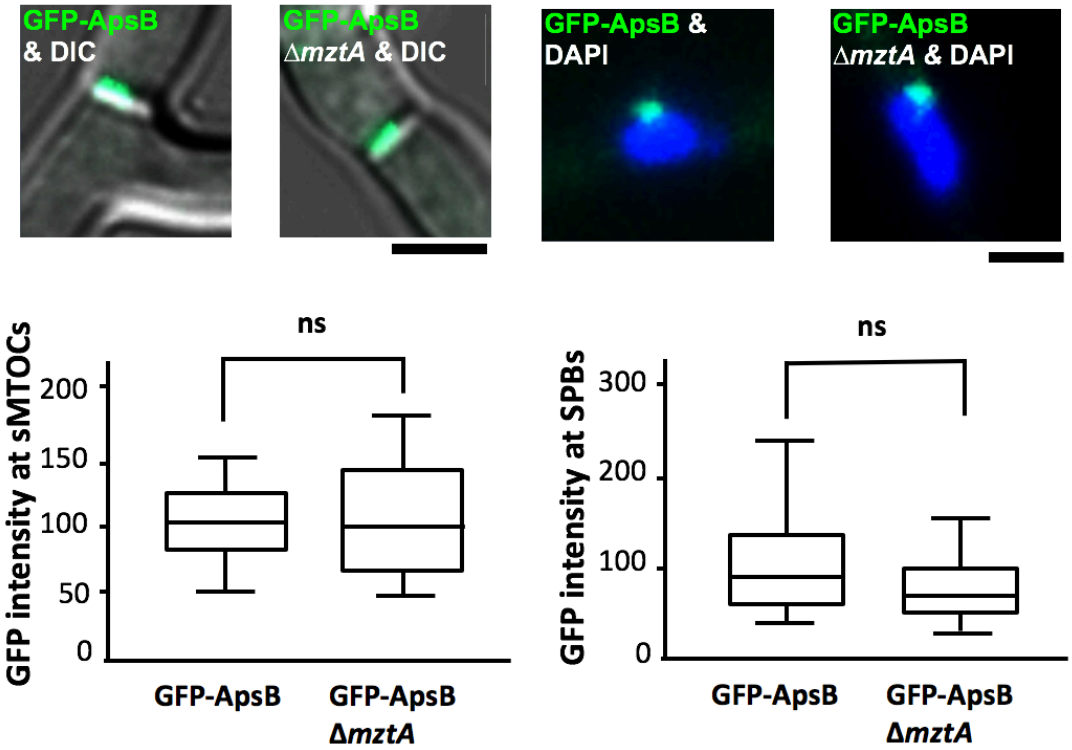

Fig. S2: ApsB localization at sMTOCs and SPBs was not affected in a *ΔmztA* strain. Strains SYZ2 (*alcA(p)::GFP::apsB*) and SXL63 (*alcA(p)::GFP::apsB*; *ΔmztA*) were incubated in MM (2% glycerol) at 28°C overnight with supplements and imaged. Nuclei were stained with DAPI. In total 30 SPBs or 30 septa were analyzed for the quantification. Images of 10-15 sections were taken along the Z-axis at 0.27-µm increments. Maximum projection images were obtained and maximum fluorescence intensities over the background intensity were used for statistical analysis. The exposure time and shutter level were set to be identical for each strain. Mann-Whitney U test was performed with GraphPad Prism 7. The boxes mark the region of the SD. The vertical lines indicate the range of all data. The ns above the graph indicate no significant differences compared to wild type ($p > 0.05$). Scale bar, 2 µm.

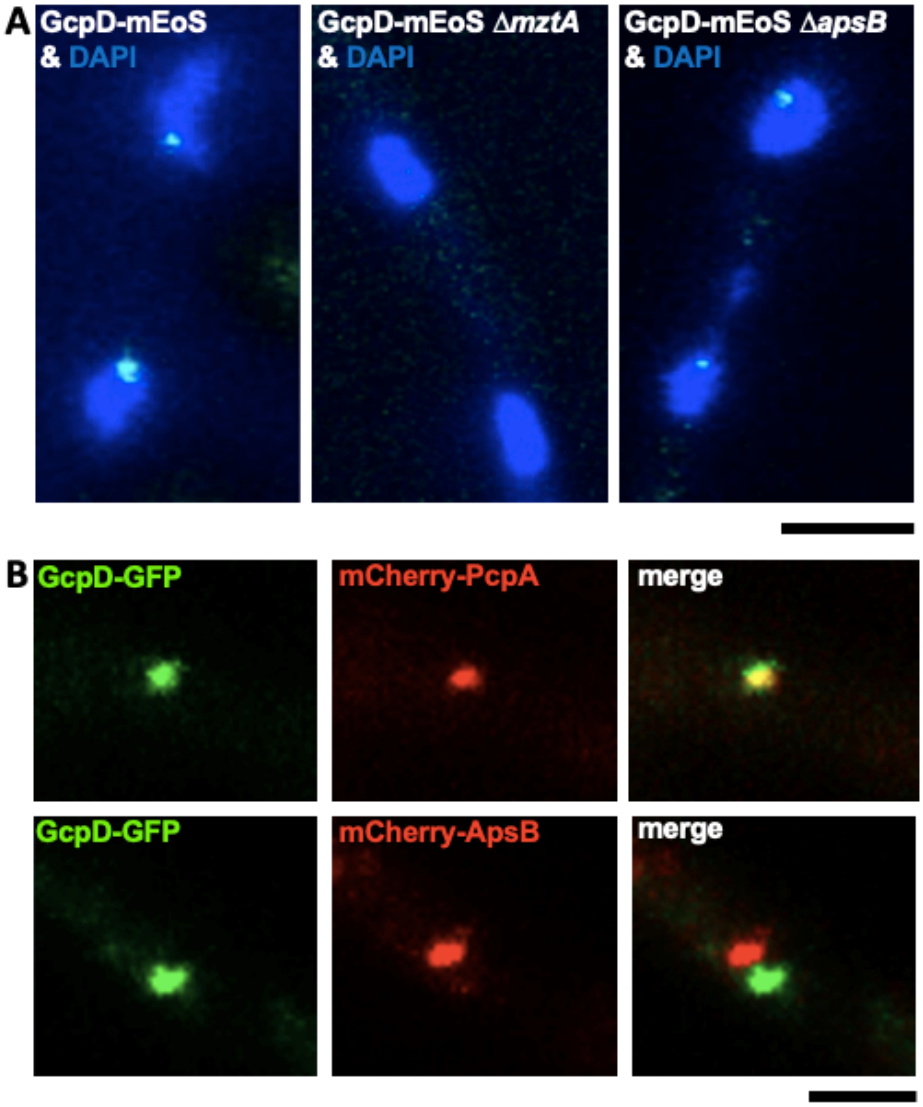

Fig. S3: Role of MztA in recruitment of the γ-TuRC-specific component GcpD and co-localization analysis of GcpD with PcpA or ApsB. (A) GcpD localization on SPBs depends on MztA but not on ApsB. Strain SXL99 (*gcpD::mEosFP*), SXL101 (*gcpD::mEosFP; ΔapsB::pyroA*) and SXL111 (*gcpD::mEosFP; ΔmztA(L)::pyroA*) were incubated in MM (2% glycerol) at 28°C with supplements overnight and observed in the GFP channel. Nuclei were stained with DAPI. Scale bar, 2 µm. **(B)** Localization of GcpD with PcpA or ApsB. Strains SXL147 (*gcpD::GFP; alcA(p)::mCherry::apsB*) and SXL148 (*gcpD::GFP; alcA(p)::mCherry::pcpA*) were incubated in MM (2% glycerol) at 28°C overnight and imaged. Scale bar, 2 µm.

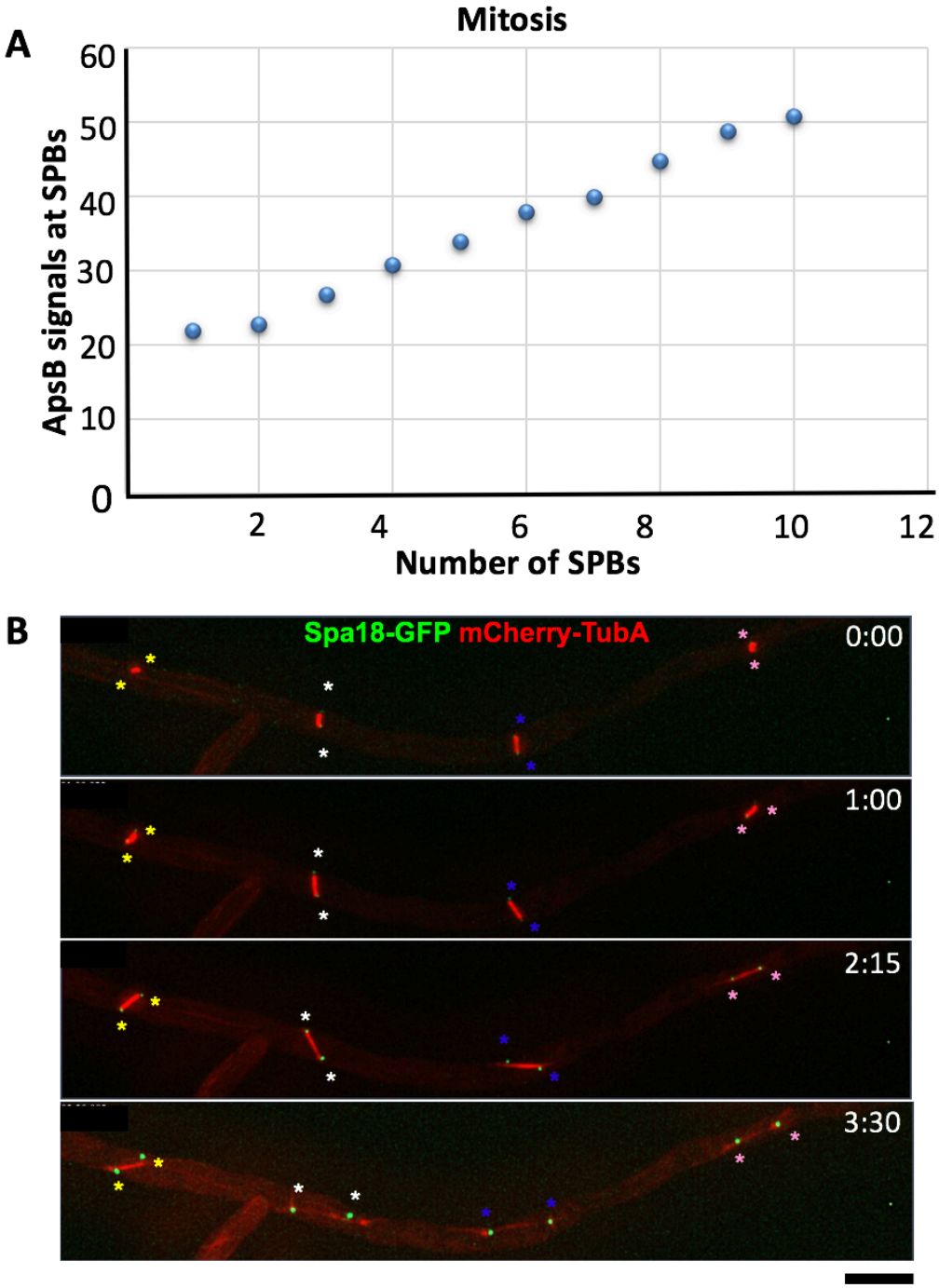

Fig. S4: ApsB and Spa18 concentrations at SPBs are increasing during mitosis. **(A)** PALM data showed increasing numbers of ApsB during mitosis. 10 SPBs were counted. Strain SXL100 (*apsB::mEoS*) was analyzed with PALM. **(B)** Spa18 started to be assembled into short spindles and gradually increasing intensities as mitosic spindles elongated. Time lapse images were taken every 1 min. Strain SXL21 was incubated in 8 well u-slides at 28°C overnight. Scale bar, 5 µm.

Table S1: List of *A. nidulans* strains used in this study.

Click here to Download Table S1

Table S2: List of plasmids used in this study.

Click here to Download Table S2

Table S3. Primers used in this work.

Click here to Download Table S3

Table S4: Molecular numbers of MTOC components at SPBs. Four MTOC components ApsB, GcpC, GcpD and MztA were quantified at SPBs and sMTOCs with super-resolution microscopy (PALM). In interphase, 32 SPBs for ApsB, 66 SPBs for GcpC, 20 SPBs for GcpD and 34 SPBs for MztA were counted. 20 septa for GcpC, 10 sepat for GcpD and 10 septa for MztA were counted at interphase. In mitosis, each protein was counted at 10 SPBs. Strains SXL114 (*mztA::mEoS*; *alcA::GFP::tubA*), SXL115 (*gcpC::mEoS*;*alcA::GFP::tubA*), SXL116 (*apsB::mEoS*; *alcA::GFP::tubA*) and SXL117 (*gcpD::mEoS*; *alcA::GFP::tubA*) were used where spindles were observed with the GFP channel. The average numbers of each protein are shown in the Table with SD. SD of interphase SPB is much higher than that of mitosis, indicating the high dynamics in interphase.

	ApsB	GcpC	GcpD	MztA
Interphase	20±8.8	31.9±22.7	10.6±4.8	30.7±12.6
Mitosis	41.6±6.6	46.7±4.2	15.6±2.6	58.6±6.0

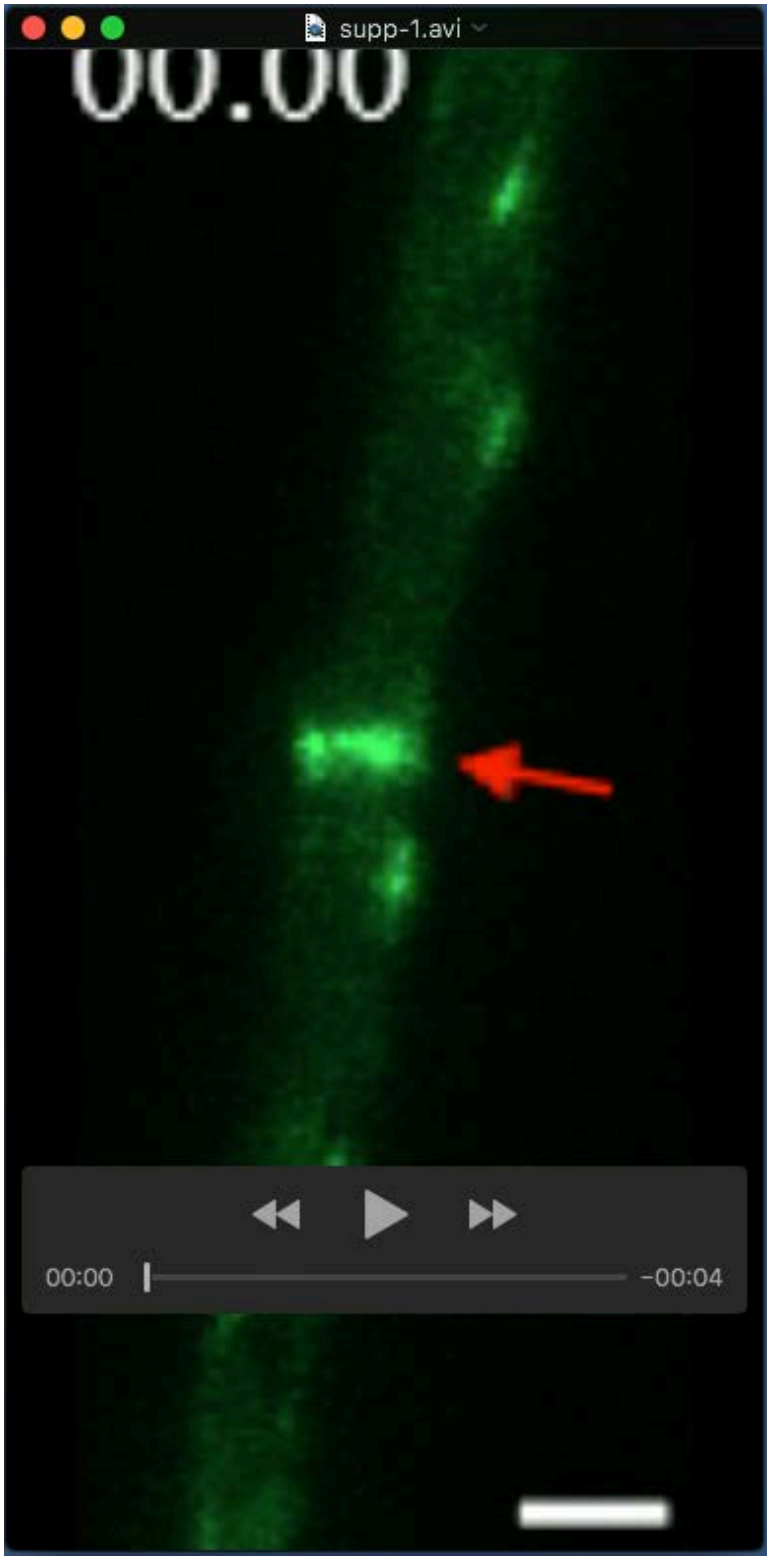

Movie 1: GFP-KipA in the mztA mutant. Germlings of strain SXL87 (ΔmztA, alcA(p)::GFP::kipA) were cultured in 8 well u-slides at 28°C overnight. 20 frames were captured every 5s and movie speed is 5fps. Arrows indicated the position of the septum. Scale bar: 2 µm.

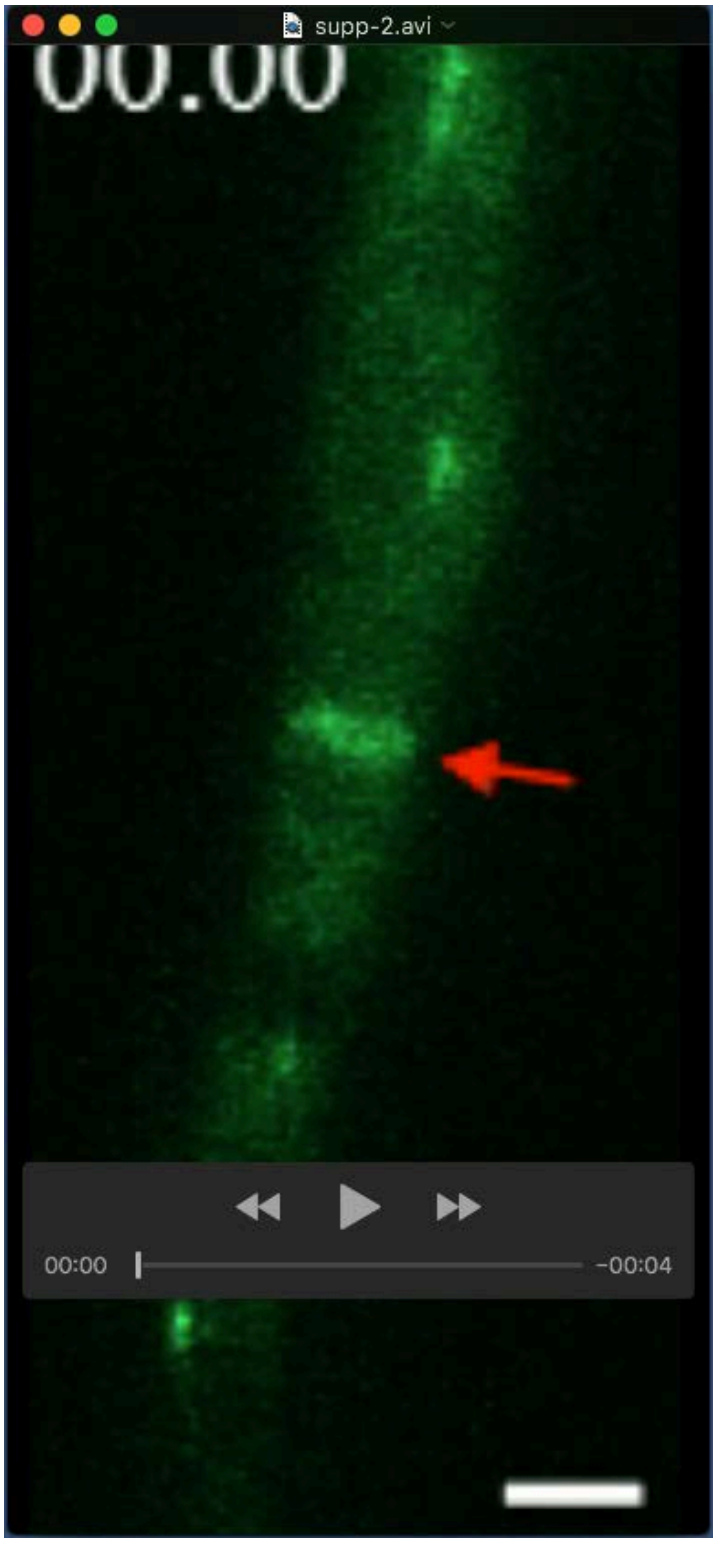

Movie 2: GFP-KipA in wild type. Germlings of strain SSH27 (alcA(p)::GFP::kipA) were cultured in 8 well u-slides at 28°C overnight. 20 frames were captured every 5s and movie speed is 5fps. Arrows indicated the position of the septum. Scale bar, 2 µm.